Probabilistic Hazard Analysis and Modelling of Tsunami Inundation for the Auckland Region from Regional Source Tsunami

Philip Gillibrand
William Power
Emily Lane
Xiaoming Wang
Julian Sykes
Hannah Brackley
Jade Arnold

Prepared for

Auckland Regional Council

By

National Institute of Water & Atmospheric Research Ltd
10 Kyle Street, Riccarton, Christchurch 8011,
P O Box 8602, Christchurch 8440, New Zealand
Phone +64-3-348 8987, Fax +64-3-348 5548, www.niwa.co.nz

and

Institute of Geological & Nuclear Sciences Ltd
PO Box 30368, Lower Hutt, New Zealand
Phone +64-4-570 14444, Fax +64-4-570 4600, www.gns.cri.nz

NIWA Client Report: CHC2010-102
NIWA Project: ARC10502
August 2010

GNS Consultancy Report 2010/200
GNS Project No.: 410W1164

Reviewed by:

Name:	**Scott Stephens**
Position	**Scientist Coastal Hydrodynamics**
Organisation:	**NIWA**
Date:	**October 2010**

Released by:

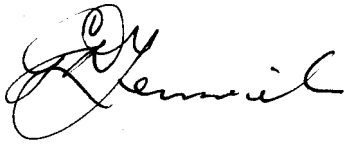

Name:	**Graham Fenwick**
Position	**Assistant Regional Manager**
Organisation:	**NIWA**
Date:	**October 2010**

Contents

1 Executive Summary

GNS and NIWA were contracted by Auckland Regional Council to assess the probabilistic inundation of the Auckland region's developed areas by regional source tsunami with an "Average Recurrence Interval" (ARI) of 2500 years. This is defined as a tsunami that is equalled or exceeded in height (or speed or some other property of tsunami) once, on average, every 2500 years. It has an Annual Exceedance Probability (AEP) of 1/2500, or 0.0004. In other words, in any calendar year there is a 1 in 2500 chance of a tsunami of 2500-year ARI height occurring.

Logic trees were constructed for New Hebrides and Kermadec Arc, the two regional tsunami sources identified as being significant to the Auckland region coastline. Initial modelling identified the Kermadec Arc as the major regional tsunami hazard for the Auckland region east coast. Both the Kermadec Arc and the New Hebrides pose a similar tsunami hazard to the ARC west coast. This hazard is considerably lower than that posed to the east coast. As the risk exposure is also lower on the west coast, the study focused on the ARC east coast.

The two source regions were each divided into a set of unit-source 'patches'. For each unit source, the tsunami propagation time-history caused by 1 m of fault slip was estimated using the COMCOT model. Using the statistical parameters for each of the 12 logic-tree branches, 100 000-year simulated sequences of earthquakes on the Kermadec and New Hebrides arcs were constructed. Each 100 000-year sequence contained about 3000 simulated earthquakes, which were modelled by COMCOT by linearly superposing unit-source simulations. The maximum water level at the Auckland region east coast was recorded for each event, and the greatest height (to the nearest metre) that was exceeded on more than 40 occasions was used to estimate the height that tsunami would reach (or exceed) once, on average, every 2500 years. The 100 largest events were selected for the purpose of full inundation modelling.

Inundation modelling for the 100 largest tsunami was undertaken using the RiCOM hydrodynamic model. The inundation model was forced by time histories of water level and current velocity extracted from the COMCOT simulations along the eastern boundary of the RiCOM model domain. Predictions of water level time series at points along 175°E, which lies in the interior of both model domains, by the two models were contrasted, and compared well. From the 100 scenarios of tsunami inundation along the Auckland coast predicted by RiCOM, probabilistic inundation depth and maximum current speed on a 2500-year time scale were determined for seven regions of Auckland: Omaha, Snells Beach to Martins Bay; Waiwera to Whangaparaoa Peninsula; Browns Bay to Devonport; Te Atatu to St Heliers, including CBD; Panmure to Maraetai; Waiheke Island (Oneroa, Surfdale, Onetangi); and Kaiaua.

Inundation was first modelled assuming that all tsunami arrived at Mean High Water Springs (MHWS). Results are presented for this set of simulations. But the study also considered the effects of the tides on the predicted inundation. The tidal state at the time of arrival of the tsunami can have a significant effect on the maximum nearshore water level and the consequent inundation. Over the 100 000-year time scale considered, tsunami will inevitably arrive at a variety of tidal heights; this variability has important consequences for the probabilistic inundation. In the study, we analyse the effect of tides on the predicted tsunami

inundation, and present results that include those tidal effects. Tidal effects are not considered for the probabilistic analysis of maximum current speeds.

The largest impact on the ARC east coast is on Great Barrier Island. Omaha, Orewa and surrounding areas also have a high risk of inundation over significant areas. Further into the Hauraki Gulf, this risk lessens as the areas are sheltered by outlying islands. In most other areas, the inundation is confined to narrow coastal strips. State Highway 1 north of Hatfields beach and at Northcote and the North-western motorway between Te Atatu and Point Chevalier are also at risk of inundation by tsunami with a 2500-year ARI.

This study presents the first probabilistic analysis of dynamic modelling of tsunami inundation for the New Zealand coast. In all, inundation of the Auckland region from 100 tsunami events has been dynamically modelled, and the results synthesized into probabilistic maps of inundation depth and maximum current speed from 2500-year ARI tsunami. The simulations conducted assumed tsunami arrival coincides with MHWS tides to provide conservative estimates of probabilistic inundation suitable for emergency management and planning. Incorporating varying tidal states provides more accurate estimates of the probabilistic inundation, but the results for the present study were hindered because the influence of smaller tsunami on the probabilistic inundation at some locations was not captured in this study. The study provides the most comprehensive assessment of tsunami inundation of the Auckland region from regional source tsunami available to date.

2 Introduction

Auckland Regional Council commissioned the Institute of Geological and Nuclear Sciences (GNS Science) and the National Institute of Water and Atmospheric Research (NIWA) to jointly undertake a probabilistic tsunami hazard analysis (PTHA) for Auckland region from regional source tsunami. The goal of the project is to provide maps of probabilistic inundation of Auckland on a 2500-year time scale. The approach taken in this project differs from previous modelling studies of tsunami inundation around New Zealand which typically have been scenario-based. For example, an earlier study of tsunami inundation of the Auckland coastline investigated the potential impacts of tsunami originating from South America (Lane et al., 2007). In that study, the inundation resulting from a single tsunami event, equivalent to the 1868 Peru/Chile tsunami, was modelled. The rationale for the study was that earthquakes along the Chile/Peru coastline pose the most likely source of tsunami to affect the Auckland coast on timescales of 100 years, and the modelled event was chosen as a "worst-case scenario", with low probability but high risk.

On longer timescales, the most potentially devastating tsunami hazard for New Zealand shores arises from local or regional sources. In this study, we examine the tsunami hazard for Auckland region from regional source tsunami. The main regional sources are the Tonga-Kermadec and Southern New Hebrides tectonic faults. In contrast to the scenario-based approach of the previous study, this study takes a probabilistic approach to the hazard. The generation and propagation of a large number of possible tsunami are modelled, and the predicted inundation from each event is recorded. The probabilistic inundation of the Auckland region on a given time scale can then be assessed, encompassing uncertainty in understanding of the geophysical source processes. We aim to improve knowledge about the probable magnitude of regional tsunami generation mechanisms over a 2500-year time scale. The 2500-year ARI is chosen for consistency with similar earthquake hazard studies. The principal outcome from the study will be maps of probabilistic inundation hazard for the Auckland region.

The overall objective of the study, therefore, is to determine the probabilistic inundation of the Auckland region's developed areas by regional source tsunami on a 2500-year time scale. This will be achieved through the following sub-objectives:

1. Perform a probabilistic regional tsunami hazard analysis for the Auckland region, identifying dominant sources of tsunami at a 2500-year ARI;
2. Model unit-source tsunami propagation using the COMCOT tsunami model;
3. Model inundation around Auckland for a range of likely source scenarios using the RiCOM hydrodynamic model, driven by boundary conditions generated by COMCOT;
4. Determine and map the probable inundation of specific urban areas of the Auckland region for tsunami at a 2500-year ARI.

The methods used to achieve each sub-objective are described in detail in the next section. In the study, we also consider the effects of the tides on the predicted inundation. Standard practise in tsunami inundation modelling studies is to model inundation at a fixed tidal state i.e. the variation in tidal height is ignored over the duration of the arrival of the tsunami and, in

order to develop conservative evacuation plans, modelling is typically performed at mean high water springs (MHWS) or an equivalent high water state. However, when the local tidal range is comparable to the height of the tsunami, as is often the case in New Zealand, the tidal state at the time of tsunami arrival can have a significant influence on the subsequent inundation. In a probabilistic analysis, therefore, when many inundation events are considered, the tidal state can have a profound influence on the probabilistic inundation. In this study, we develop a method to include the tidal state at the time of tsunami arrival into the probabilistic analysis. These results are presented in addition to the standard case of modelled inundation at MHWS.

3 Methods

The purpose of this work is to produce a set of tsunami boundary conditions that can be applied to model tsunami inundation at selected locations along the Auckland Regional Council coastline, and to determine the probabilistic inundation on a 2500-year time scale.

This work is accomplished in the following stages:

- Statistical characterisation of appropriate source regions, taking uncertainty into account in a logic tree framework.
- Geometrical modelling of the source fault planes
- Modelling of unit-source tsunami propagation
- Estimation of the 2500-year ARI tsunami hazard for each logic-tree branch
- Selection of the 84-percentile logic tree branch
- Selection of scenarios for inundation modelling
- Creation of boundary conditions for inundation scenarios
- Preparation of high-resolution inundation grids
- Modelling inundation for selected scenarios
- Collation of inundation scenarios into probabilistic inundation and max speed
- Incorporation of tides into probabilistic inundation

3.1 Regional Source Tsunami Hazard Estimation at the 2500-year ARI 84-Percentile Level and Selection of Stochastic Scenario Ensemble for Inundation Modelling

The primary regional sources of interest for the ARC area are the Kermadec Arc, a subduction zone that extends northwards from East Cape to the point where it intersects the Louisville Ridge; and the southern New Hebrides Arc a subduction zone that lies between the southern New Hebrides and Fiji. These were judged to be the only regional sources capable of influencing the location of the 2500-year ARI 84-percentile inundation line in the ARC region. The 2500-year ARI inundation line is the boundary between those areas that are expected to be inundated by tsunami at least once, on average, every 2500 years, and those that are not. The 84^{th} percentile of uncertainty is a measure of confidence in the result, bearing in mind the uncertainties in the parameters that determine the tsunami hazard. Specifically, it means that we have 84-percent confidence that the true 2500-year ARI inundation line lies closer to the coast than the one we have drawn. The 84^{th} percentile is used because it represents the mean plus one standard deviation of uncertainty (in a normal distribution), in a sense we can view an

inundation line drawn at the 84th percentile of uncertainty as representing the upper end of an error bar around an estimate of the true 2500-year ARI inundation line.

Evaluation of the available geodetic, geological, and seismic data was used to produce logic-trees for each of the two source zones (Power et al., 2010). It was judged that the most important parameters controlling the magnitude (size) and frequency (how often) distribution of tsunami-generating earthquakes in the two source regions were the maximum moment magnitude, Mw, of an earthquake that the source region could generate, and the seismic coupling coefficient, C, which represents the proportion of the plate convergence rate released seismically (loosely speaking it is a measure of the 'stickiness' of the boundary between the tectonic plates). Because the actual values of these parameters are not known logic-tree branches are created corresponding to the range of different values that are possible, and then a weighting (shown in brackets) is attached to each branch corresponding to the assessed likelihood (Figures 1 and 2). This weighting is based on expert opinion, in this case that of the authors of Power et al (2010), after reviewing the available data. These weightings cannot be derived from first principles, and different experts may come to a different set of weightings; furthermore, the weightings can be expected to change in future as additional scientific information becomes available regarding the earthquake source zones. Power et al (2010) mention two circumstances likely to result in a revision of the weightings associated with the Kermadec Arc: if additional geodetic data (on top of the current GPS measurements for Raoul Island) were to show strong coupling on the plate interface, or if additional evidence were to link a large paleotsunami which hit northern New Zealand in the 15th century (Goff et al, 2010) to a subduction zone earthquake source. Either of these would lead to revision of the logic tree, probably leading to a rise in the estimated tsunami hazard to the Auckland region associated with a 2500-year ARI.

Figure 1

Logic tree for the Kermadec Arc.

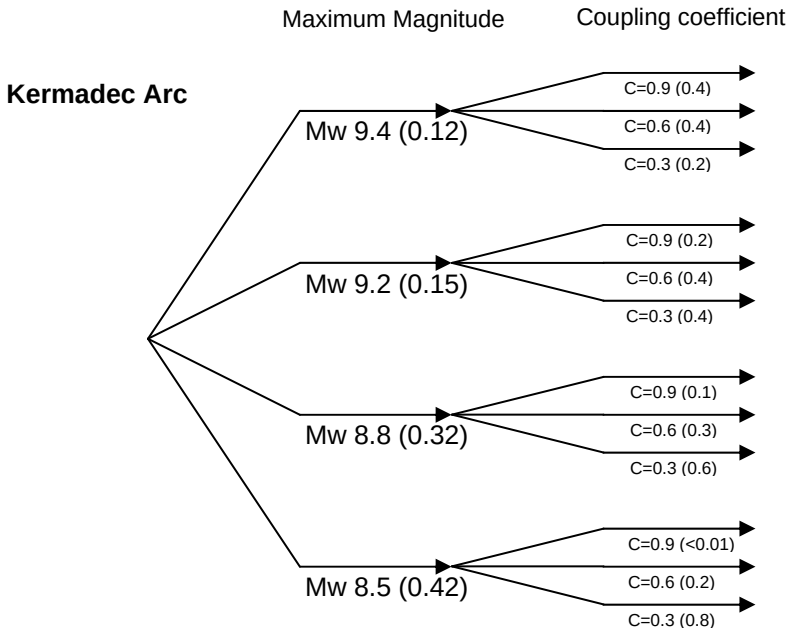

Figure 2

Logic tree for the Southern New Hebrides.

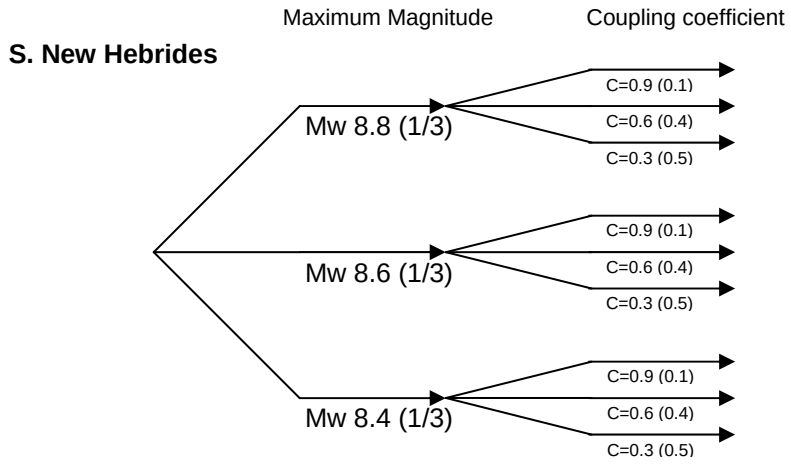

The two source regions were each divided into a set of unit-source 'patches' 100 km long and either 50 km (Kermadec Arc) or 60 km (New Hebrides) wide (Figures 3 and 4). The geometry of these patches was estimated from seismic data (Power et al, 2010).

Figure 3

Unit source locations for Kermadec Arc.

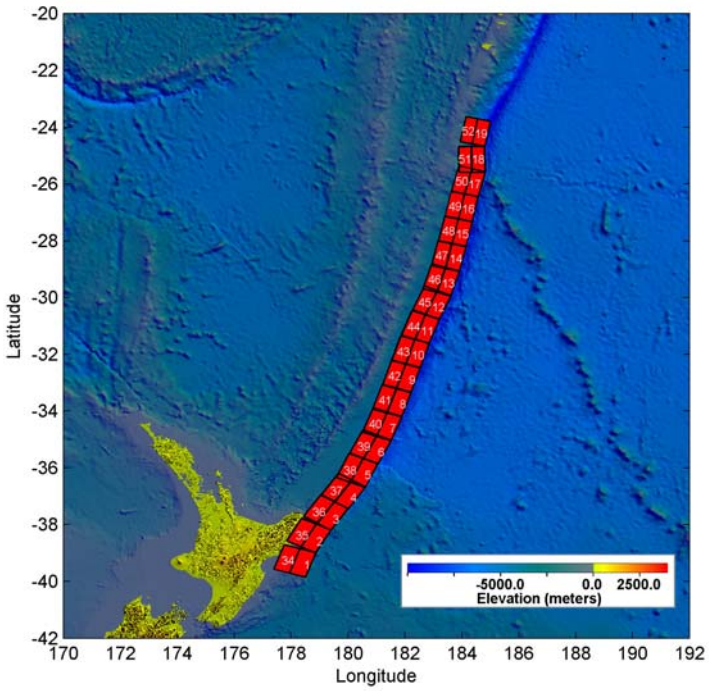

Figure 4

Unit source locations for southern New Hebrides.

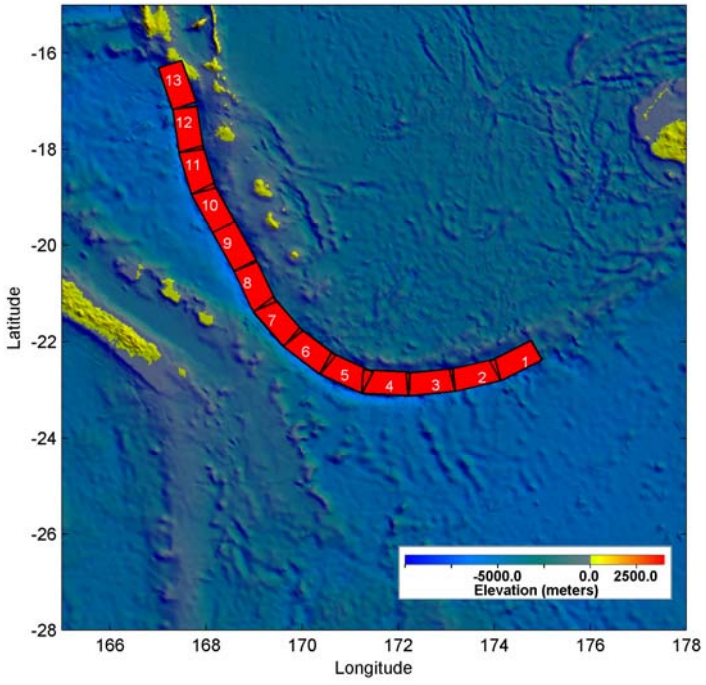

For each unit source, the tsunami propagation time-history caused by 1 m of fault slip was estimated using the COMCOT model (Wang, 2008; see Section 3.2). The nested grid structure used for this modelling is illustrated in Figure 5. The linear form of the tsunami equations were used which is appropriate for applying the superposition principle to the unit source models. However, this linear approximation limits the accuracy of the models in shallow water.

The unit-source time histories can be used to estimate the tsunami wave fields for earthquakes with a wide variety of different slips and rupture lengths using the superposition principle. A weighted sum of the unit-source wavefields is used to estimate the wavefield caused by the full rupture. For example, if an earthquake rupture was to occur spanning a single unit-source area, but with 2 m of slip, the resulting tsunami could be estimated simply by doubling the water levels from the pre-calculated 1 m slip unit-source. In this way it is possible to estimate the tsunami affects of a wide range of scenario earthquakes much more quickly than if each scenario had to be modelled *ab initio*.

In laymans-terms, the idea behind the unit sources is that they can be used as basic building-blocks which can be combined to quickly create simulations of tsunami created by larger and longer earthquake ruptures.

Figure 5

Nested grid structure used for tsunami propagation modelling. Grid resolutions are - 2 arc-minutes (about 3.0 km) for Layer 01, 30 arc-seconds (about 750 m) for Layer 02, 10 arc-seconds (about 250 m) for Layers 03 and 04. The yellow boxes indicate the coverage of nested grid layers.

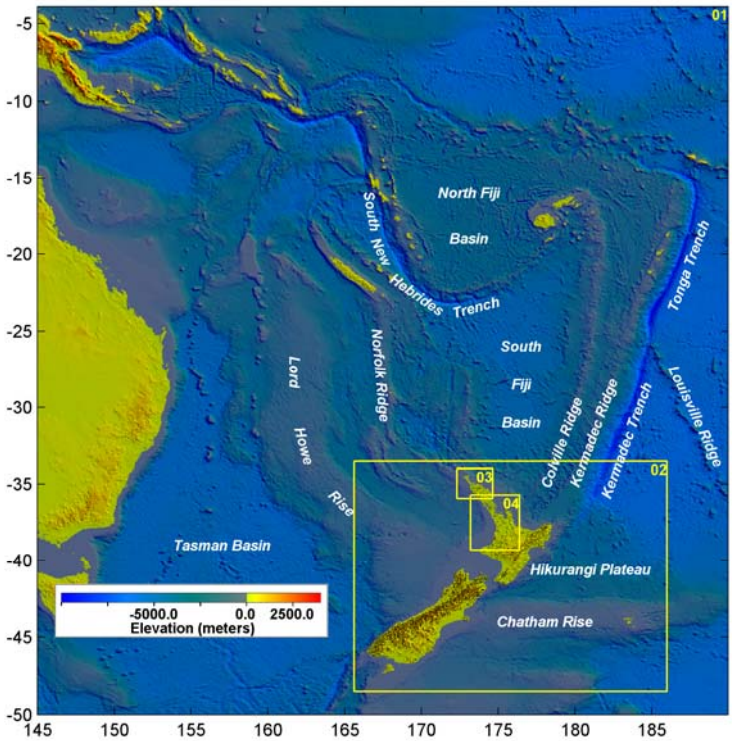

The results from unit source calculations were used to analyse the relative importance of tsunami impacts from different earthquake scenarios, and also to provide offshore boundary

conditions to the RiCOM model to simulate the subsequent nearshore shoaling, run-up and inundation on land. The sensitivity of the results to the location of the source is discussed in Appendix 1.

Time series of model-predicted water level and velocity were stored on a 2 arc-minute grid over the area from 165.6 to 186.0°E and from 48.5 to 23.5°S.

Water level time-series predictions were also stored on a 30 arc-second grid over the area from 172.3 to 176.4°E and from 39.3 to 34.0°S. To conserve disc space only data points within 3 km of the coast were stored.

Starting with the Kermadec Arc, a 100 000 year simulated sequence of earthquakes on the Kermadec Arc was calculated according to the statistical parameters for each of the 12 logic-tree branches. The maximum water level was recorded for each simulated event, and the greatest height (to the nearest metre) that was exceeded on more than 40 occasions was used to estimate the 2500-year ARI hazard for that branch.

The maximum water-level results produced for each branch of the logic-tree were placed in order according to their impact on the Auckland region. Taking the weightings for each branch into account, the particular branch corresponding to the 84^{th} percentile of uncertainty was selected. This means that if the selected branch is used to perform the tsunami hazard calculations, then we can have 84 percent confidence that the true hazard is no greater than that estimated using the chosen branch. The reason for using the 84^{th} percentile is that it corresponds to the mean plus one standard deviation of uncertainty (in a normal distribution). This is similar to using the upper bound on an error bar. Figure 6 shows the estimated hazard posed by that branch of the logic tree.

An identical process was followed to arrive at the 2500-year ARI tsunami hazard from the southern New Hebrides (Figure 7).

Analysis of Figures 6 and 7 demonstrates that the Kermadec Arc is a significantly greater hazard for the Auckland region east coast, where most of the exposure to tsunami risk is located. For the Auckland region west coast, the hazard from the two sources is comparable at the 2500-year ARI 84 percentile level (this is not necessarily true at other return times and confidence levels). Because of the reduced hazard on the west coast, coupled with the lower exposure to tsunami risk there, the rest of this study focuses on the tsunami hazard to the Auckland region east coast.

These hazard plots are based on linear modelling of the tsunami. Nonlinear processes change the shape of large amplitude tsunami waves in shallow water, leading to a more steeply-fronted wave. Nonlinearities also change the frequency spectrum of the tsunami wave and may alter resonant interactions with the coast.

The combined coastal hazard from both sources cannot in general be simply obtained from the hazard plots for each individual source. However, for the Auckland region east coast the hazard from the Kermadec source is significantly higher than from the southern New Hebrides. The 2500-year ARI 84 percentile water-level for the Auckland region east coast is higher than that of the maximum event possible from the southern New Hebrides in our logic tree. Consequently for the east coast we may take the maximum water levels in Figure 6 as representing the 2500-year ARI 84 percentile hazard from all regional sources.

Using the logic-tree branch for the Kermadec arc that was estimated to represent the 84 percentile uncertainty at 2500-year ARI, a synthetic sequence of tsunamigenic earthquakes was created for a 100 000 year period. The magnitude of each event was randomly selected according to the statistical properties of the chosen branch. The midpoint location of each rupture was randomly selected, and the length of rupture determined according to the scaling laws presented in Power et al. (2007), with a maximum source width of 100km.

Over this 100 000 year period there are approximately 3000 simulated earthquakes, and for each of these the unit-source models were used to estimate the subsequent maximum water levels around the coast. For each event, the spatial average of the maximum water levels reached at all points around the Auckland region coast was calculated (using a strip extending up to 3km from the shoreline, but not including the Great and Little Barrier Islands). The events were then ranked from that with the highest (average) water level on the Auckland region shoreline to that with the lowest. From this ranking, the 100 largest events were selected for the purpose of inundation modelling.

Figure 6

Estimated 2500-year ARI 84 percentile tsunami hazard from the Kermadec Arc, expressed in terms of the maximum water level in metres.

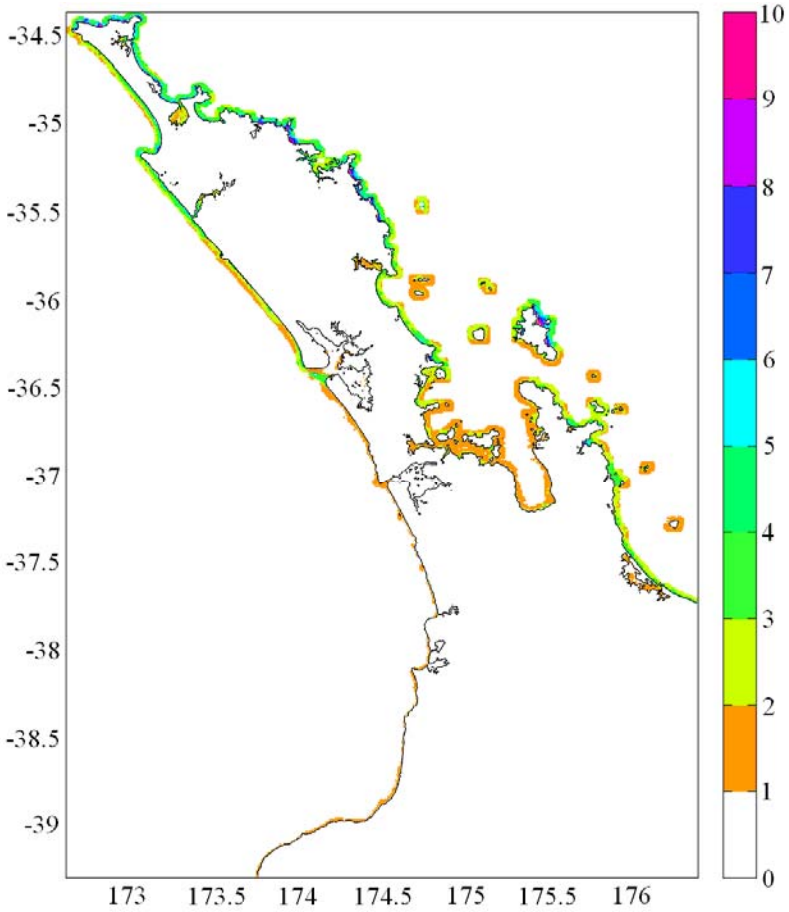

Figure 7

Estimated 2500-year ARI 84 percentile tsunami hazard from the southern New Hebrides, expressed in terms of the maximum water level in metres.

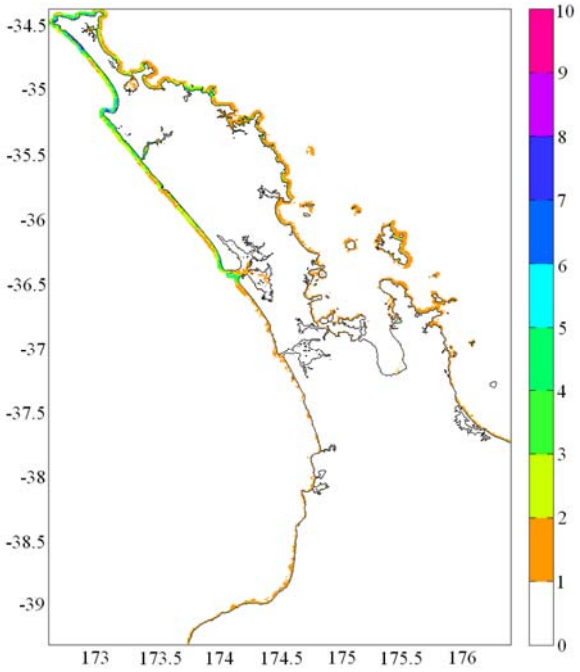

3.2 Unit Source Modelling: The COMCOT Model

The generation and propagation of tsunami from unit sources are modelled via an in-house tsunami model - COMCOT (Cornell Multi-grid Coupled Tsunami model). COMCOT uses a modified leap-frog finite difference scheme to solve (linear and/or nonlinear) shallow water equations in a staggered nested grid system. The model is capable of simulating the generation, propagation and the subsequent runup and inundation of tsunami from either local or distant sources. It has been systematically validated against analytical solutions, experimental studies and typical benchmark problems (Liu et al., 1995; Cho, 1995; Wang et al., 2008). And it also has been successfully used to investigate several historical and recent tsunami events, such as the 1960 Chilean tsunami (Liu et al., 1994) and the 2004 Indian Ocean tsunami (Wang and Liu, 2006, 2007; Wang, 2008). With the implementation of two-way nested grid coupling, COMCOT simultaneously calculates the tsunami propagation in the deep ocean with a relatively larger spatial resolution and the runup and inundation process in the targeted coastal zones with a finer spatial resolution.

In this study, three levels of nested grids are implemented to model the propagation of tsunami in the deep ocean, over continental shelf and nearshore, in order to account for the shortening of tsunami waves as they shoal over the continental shelf. The first level grids (i.e., Layer01 in Figure 5) enclose the entire region of New Zealand, Kermadec-Tonga Trench and south New Hebrides Trench, ranging from 145°E to 190°E in longitude and from 50°S to 4°S in latitude, with a spatial resolution of 2 arc-minutes (about 3.0 km, from NGDC ETOPO2

database). The second level grids (i.e., Layer02) cover the entire New Zealand, including the continental shelf, and have a spatial resolution of 30 arc-seconds (about 750.0 meters, from GEBCO30 database). And the third level grids (i.e., Layer03 and 04) have a spatial resolution of 10 arc-minutes (about 250.0 meters, mainly interpolated from LINZ charts), covering Northland, ARC and the nearshore region. This type of nested grid system guarantees that the grid resolution is sufficient to resolve tsunami wave profiles both in the deep ocean and nearshore.

The elastic finite fault theory (Okada, 1985) is adopted to calculate seafloor displacement of each unit source with 1.0-meter "unit" slip. This displacement is considered the source of tsunami generation and is used as the initial condition for tsunami propagation modelling.

A database of tsunami wave field results was constructed from the results of modelling each of the 1 m slip unit sources. For a given earthquake scenario rupturing a certain area consisting of one or more unit sources, the tsunami wave fields from each of the unit sources are weighted and summed together to represent the tsunami wave field from the full rupture area. In this way it is possible to estimate the tsunami affects of a wide range of scenario earthquakes much more quickly than if each scenario had to be modelled *ab initio*.

To couple COMCOT with the RiCOM model, time histories of water level and current velocity describing the tsunami propagation from each unit source (with 1.0-meter slip) at the eastern boundary locations of the RiCOM model grid are extracted from the COMCOT simulations. The time history data from unit sources are weighted, linearly superimposed together and are then used to force the RiCOM model as boundary conditions for the inundation modelling of the top 100 scenarios.

In simple terms, the unit source models were used as basic building blocks from which simulations of larger and longer tsunami could be quickly constructed. For our selected logic tree branch this included earthquake ruptures of up to 1000km long with up to 16 meters of slip. The results of the 100 largest of these simulations were then used to provide boundary condition inputs to RICOM for inundation modelling.

3.3 Inundation Modelling

The numerical model used in this study is a general-purpose hydrodynamics and transport model known as RiCOM (River and Coastal Ocean Model). The model has been under development for several years and has been evaluated and verified continually during this process (e.g. Walters and Casulli, 1998; Walters, 2005; Walters et al., 2006a, b, c). The hydrodynamics part of this model was used to derive the results described in this report.

To permit flexibility in the creation of the model grid across the continental shelf, finite elements are used to build an unstructured grid of triangular elements of varying-size and shape to represent the model domain. The principal benefit of using unstructured meshes is to allow increasing spatial resolution (decreasing element size) in areas of shallow bathymetry or complex coastlines without the need for grid nesting. A brief description of the model RiCOM and the construction of the inundation grids are given below.

3.3.1 The Inundation Model: RiCOM

The hydrodynamic model is based on a standard set of equations - the Reynolds-averaged Navier-Stokes equation (RANS) and the incompressibility condition. In this study the hydrostatic approximation is used, so the equations reduce to the shallow water equations.

The time intervals that the model solves for are handled by a semi-implicit numerical scheme that avoids stability constraints on wave propagation. The advection scheme is semi-Lagrangian, which is robust, stable, and efficient (Staniforth and Côté, 1991). Wetting and drying of intertidal or flooded areas occurs naturally with this formulation and is a consequence of the finite volume form of the continuity equation and method of calculating fluxes (flows) through the triangular element faces. At open (sea) boundaries, a radiation condition is enforced so that outgoing waves will not reflect back into the study area, but instead are allowed to realistically continue "through" this artificial boundary and into the open sea. The equations are solved with a conjugate-gradient iterative solver. The details of the numerical approximations that lead to the required robustness and efficiency may be found in Walters and Casulli (1998) and Walters (2005).

The inundation simulations were forced by the time histories of water level and current velocity extracted along the eastern edge of the RiCOM model domain from the COMCOT simulations of tsunami propagation. The incident wave conditions were specified with a radiating boundary condition, allowing reflections from the coast of New Zealand to pass out through the eastern boundary without distorting the incident wave signal. Radiating boundary conditions were also applied along the northern, western and southern boundaries of the RiCOM grid, preventing spurious reflections back into the model domain.

Bed friction in RiCOM is treated using a quadratic stress law (i.e. stress is proportional to the square of the near-bed current velocity). The drag coefficient, C_D, is able to vary spatially. In deep water, C_D has a value of 0.0025, typical of deep sea conditions. In shallow water less than 4 m depth, a power law is applied to enhance the bed stress by up to a factor of four. This recognises the increased frictional stresses acting on flows over very shallow bathymetry and on previously dry land. This approach has been developed over a number of years to improve the performance of the model relative to historical and palaeo-tsunami data (e.g. Walters et al., 2006c).

3.3.2 The Inundation Grid

The unstructured model grid is a mesh composed of triangular elements of variable size. The grid has a number of requirements to ensure that model calculations will be accurate and free from excessive numerical errors (Henry and Walters, 1993). The primary requirements are that the triangular elements are roughly equilateral in shape and their grading in size is smooth from areas of high resolution (small elements) in the coastal zone and on land grids to areas of low resolution (large elements) offshore. The grid was generated using the programs GridGen (Henry and Walters, 1993) and TriQGrid according to the requirements described above. Layers of elements were generated along the boundaries using a frontal marching algorithm (Sadek, 1980). The size of the triangles was graded as the water depth shoaled. Once a satisfactory computational grid was created and quality assurance test were performed, water depth and land elevation values were interpolated at each node from reference datasets.

The model grid (Figure 8) covers the region from 170.5 E to 177.2 E and from 38.2 S to 28 S on the western edge of the grid and 26.5 S on the eastern edge. The spatial resolution of the grid is approximately 2km in deep water at the outer edge of the grid grading in to several hundred metres in the shallow coastal areas, and then to tens of metres in the areas where inundation modelling is to be predicted. Model bathymetry was interpolated from a combination of ETOPO1 for the deep water, blending in to NIWA regional and coastal data sets in the shallower coastal waters around New Zealand.

Inundation is modelled by creating a grid of land topography for each area, and merging it into the bathymetric grid, providing a seamless transition from ocean onto land. The topography of the land grids is taken from LiDAR (Light Detection and Ranging) data provided by Auckland Regional Council. Raw LiDAR data typically have a spatial resolution of 2 m and a vertical accuracy of about 10 cm. For the model grid, the bare earth LiDAR topography data are gridded, with a spatial resolution of about 10 m, into a number of land grids for the areas of interest. These land grids are then merged into the ocean grid. The high spatial resolution of the land grids generates a high computational demand for inundation modelling, and imposes a practical limit on the extent of land which can be included in a single computational grid. For the current study, two grids were created in order to limit the number of elements in each grid to manageable levels. Each grid consisted of more than 1.5 million triangular elements and contained a number of land areas, grouped into 'central' and 'distal' areas of Auckland region. Magnified views of the Auckland region in the two model grids are shown in Figure 9.

3.3.3 COMCOT – RiCOM Comparison

In order to test the efficacy of the coupling between COMCOT and RiCOM to drive the inundation simulations, predictions of water level by both models at grid points along a line of fixed longitude, chosen to be 175°E, were compared. The comparison focussed on the first few incoming waves only (before reflections from the coast created added complexity) and in water depths greater than 200 m, so that differences between the models due to shallow water effects were excluded (as the 'deep water' model, COMCOT was run without friction). Here we show results from the two models for scenarios 1 and 85 (out of 100): Scenarios 1 and 85 represent two distinct rupture areas, the lower half and the upper half of the Kermadec subduction interface, respectively. Therefore, they are the best candidates to reveal any difference between the results of the two models. Figures 10 and 11, time series taken from four selected locations along 175°E are presented. In Figure 12, the maximum wave heights over the entire simulation as a function of latitude for the two scenarios are shown.

Figure 8

The Auckland region tsunami inundation model grid. The grid is made up of triangular elements. Water depth (m) at each element relative to mean sea level is indicated by the colouring. The size of the elements ranges from 5 m in the inshore areas where inundation is predicted to 5 km in the outer reaches of the grid.

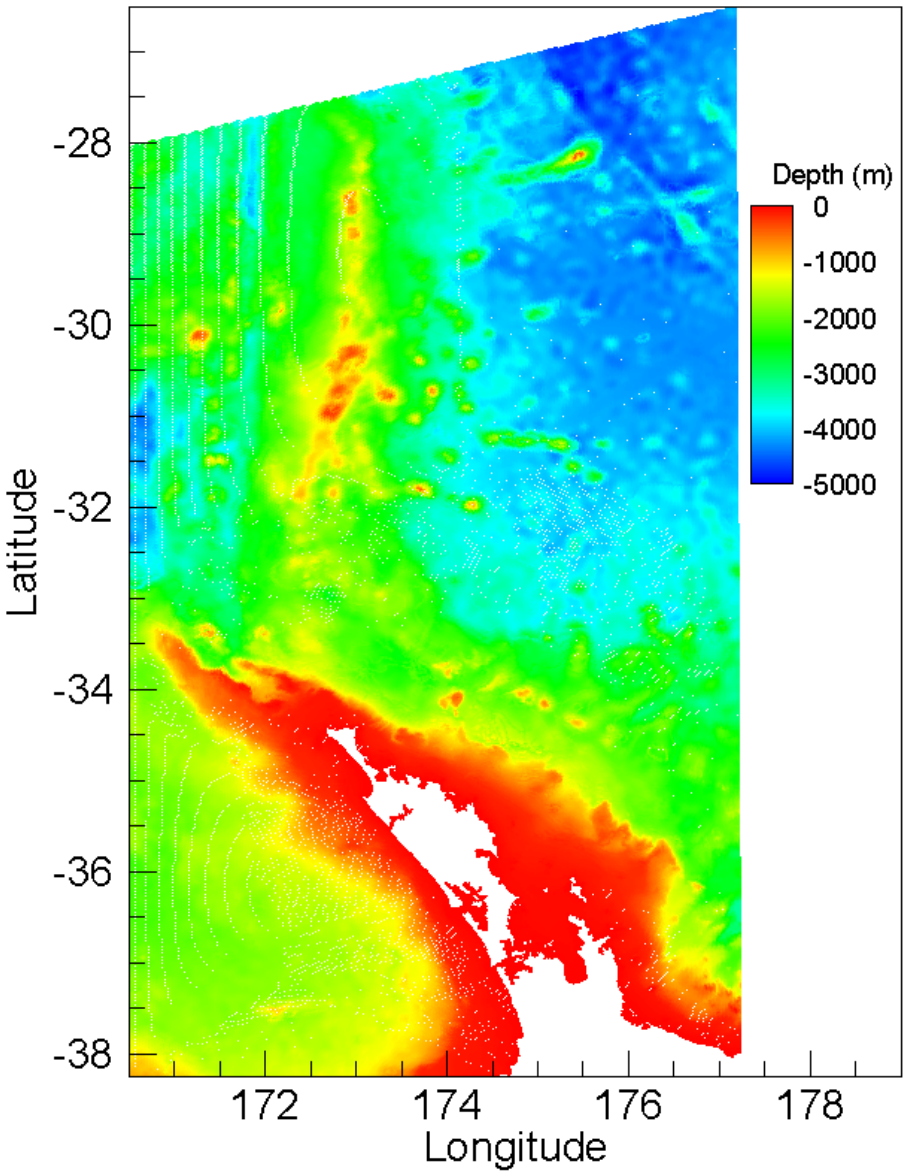

Figure 9

Magnified views of the model grids around Auckland. Individual triangular grid elements are coloured according to the elevation (m) of the seabed or land surface relative to mean sea level. The triangular elements reduce in size towards the coastline, evidenced by the solidifying of the colouring. Top: Inundation grid for central areas of Auckland. Bottom: Inundation grid for distal areas of Auckland.

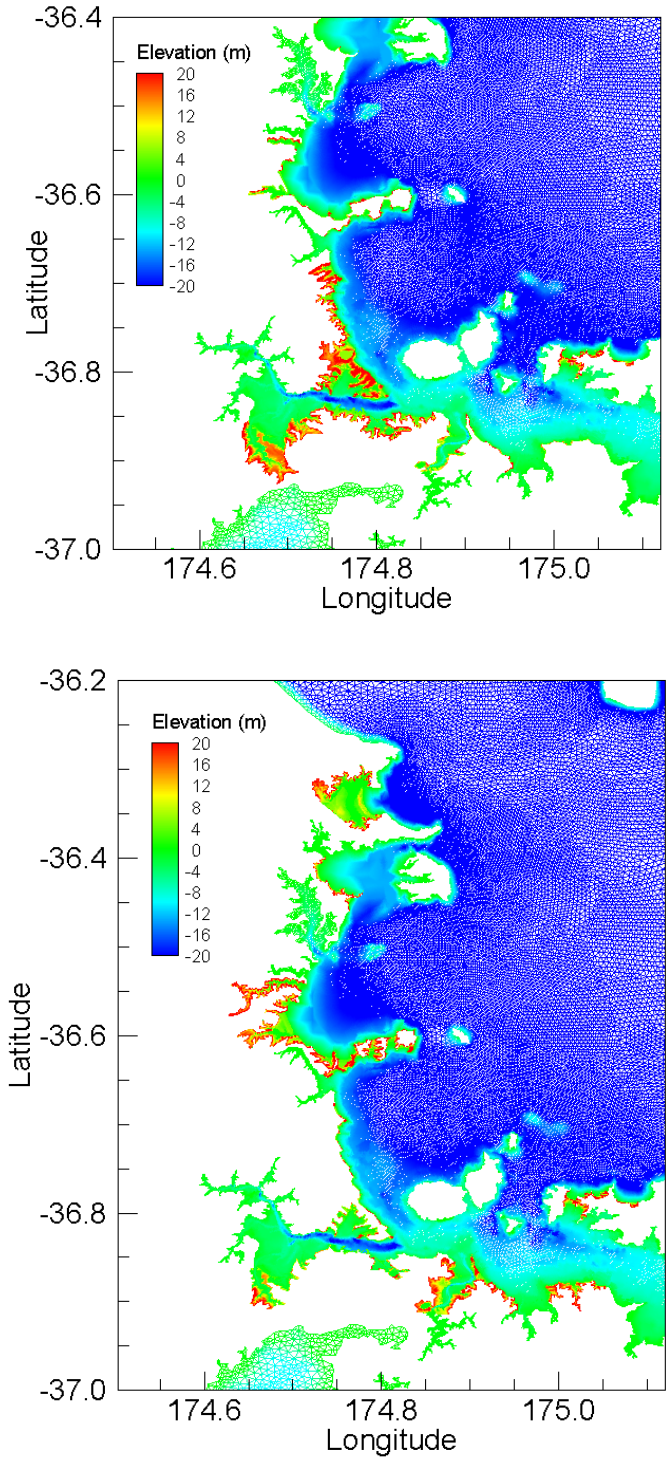

Figure 10

Comparison of water level time series (m) for RiCOM and COMCOT for Scenario 1 at four virtual gauges located at longitude 175 E and latitudes (a) 27.1 S; (b) 30.3 S; (c) 32.0 S; and (d) 34.6 S.

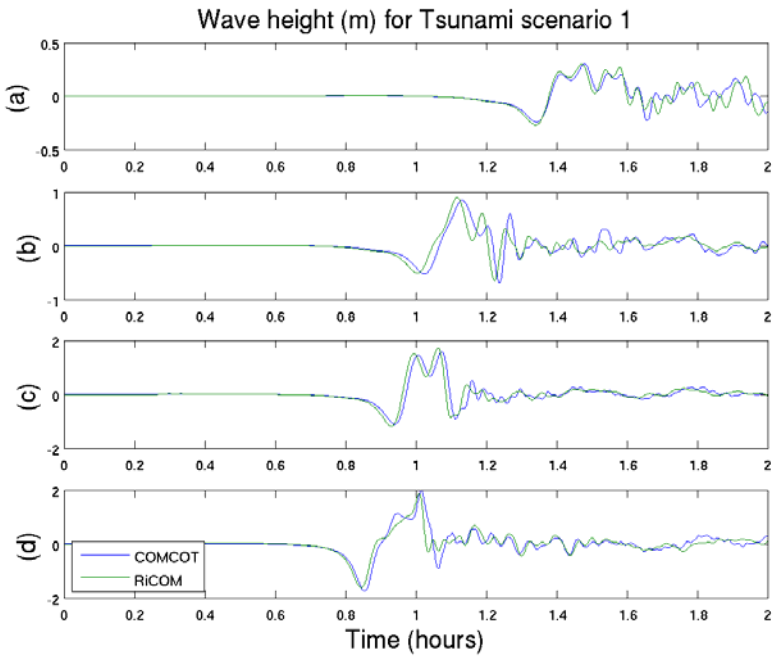

Figure 11

Comparison of water level time series (m) for RiCOM and COMCOT for Scenario 85 at four virtual gauges located at longitude 175 E and latitudes (a) 27.1 S; (b) 30.3 S; (c) 32.0 S; and (d) 34.6 S.

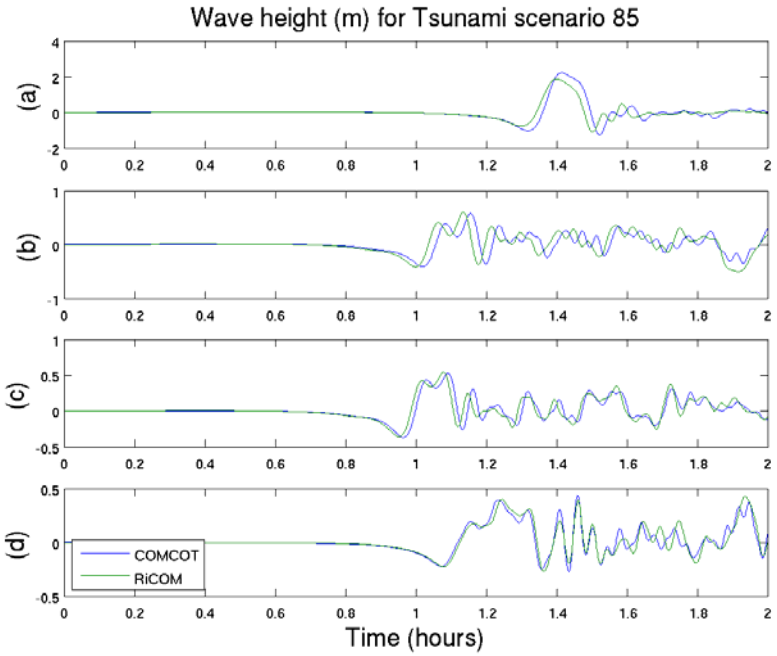

Figure 12

Comparison of maximum wave heights (m) for RiCOM and COMCOT for scenarios 1 and 85 at virtual gauges located on a line along longitude 175 E.

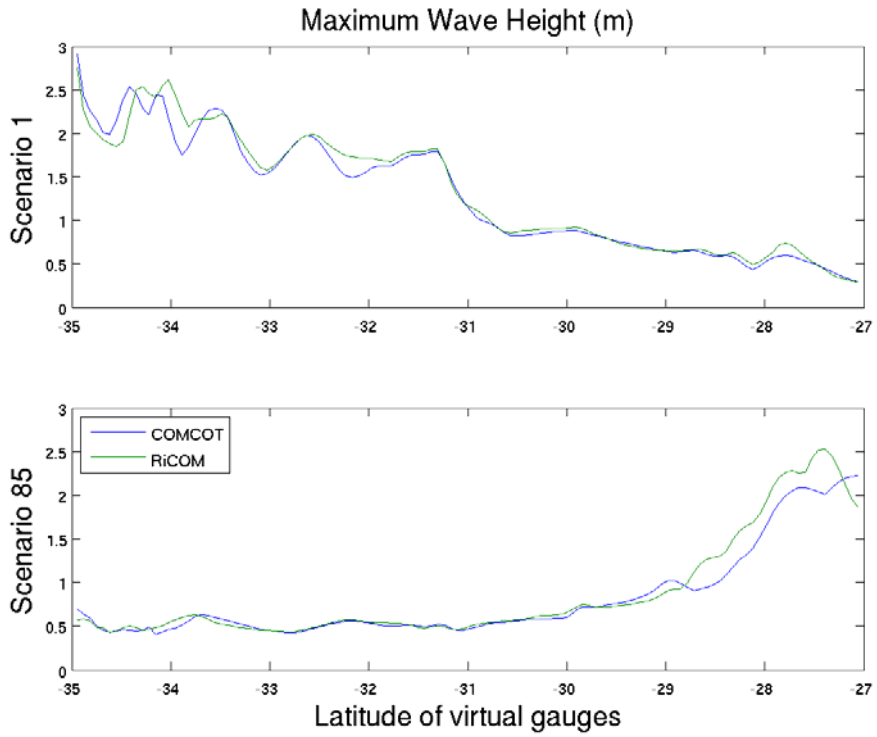

The figures demonstrate good agreement between the two models in terms of both maximum wave height at each location and the timing of the maximum wave. Inevitably there are differences between the model predictions, due to the different grids, discretizations, model numerics and configurations. Nevertheless, the comparisons in Figures 10-12 demonstrate that the models are making mutually consistent predictions of wave heights off the Auckland coast, which provides confidence in the predictions of coastal inundation.

3.4 Probabilistic Analysis of Inundation

For each of the one hundred simulations performed, the maximum inundation depth and maximum speed for each point in the model domain is recorded. This information is used to calculate the annual exceedance probabilities of tsunami inundation as discussed below. Annual exceedance probabilities can also be calculated for maximum speed. Below we discuss a methodology for also incorporating tidal state at the tsunami arrival time into the calculations. Because tidal and tsunami current speeds are considerably more spatially variable than water levels, this new technique does not work for maximum speed calculations, and the annual exceedance probabilities for speed presented in this study do not include the effects of tides.

3.4.1 Monte Carlo Simulation of Annual Exceedance Probabilities excluding Tides.

Assume that you have run N scenarios which represent a Monte Carlo simulation of all (or at least the biggest) tsunami significantly impacting the region within an *L* year period (where *L* is sufficiently large). From this you have the inundation depths at each point, ***x***, viz. $I_i(x), i = 1, \cdots N$. The probability that a given point x_0 will be inundated to greater than depth h_0 within a given year is then:

$$P(\max_{\text{annual}}(I(x_0)) > h_0) = \frac{1}{L}\sum_{i=1}^{N}\left[I_i(x_0) > h_0\right] \text{ where} \left[f\right] = \begin{cases} 1 \text{ if } f \text{ is true} \\ 0 \text{ if } f \text{ is false} \end{cases}.$$

So, for the 1:L_0 year exceedance of h_0 inundation area (i.e. the area which is expected to be inundated by a tsunami to a depth of h_0 at least once every L_0 years), we need to find

$$\left\{ x : P(\max_{\text{annual}}(I(x)) > h_0) \geq \frac{1}{L_0} \right\}.$$

In the case modelled here, we have a representative sample of one hundred tsunami that have the largest impact on the east coast of the Auckland region over 100 000 years. Thus *N* = 100 and *L* = 100 000. We wish to find inundation exceedances for 2500-year ARI and so, for each point, we sum up how many times inundation exceeds a set level h_0. If this is greater than L / L_0 = 100 000 / 2500 = 40, then that point is expected to inundate to that level at least once, on average, every 2500 years. Inundation exceedances for h_0 = 0.1, 0.5, 1.0, 1.5, 2 and 2.5 m were calculated.

These inundation scenarios were calculated with the assumption that the maximum wave height arrived at MHWS as a simple way of incorporating the tides into the calculations. In the case of moderate-amplitude tsunami, the point in the tidal cycle where the tsunami arrives can have a significant effect on the actual sea level that occurs and hence the actual inundation that results. Below we outline a method to incorporate tidal effects into the calculations.

3.4.2 Monte Carlo tsunami simulations including tides

Give sufficient computing power, tides could be added into the Monte Carlo simulations by brute force (i.e. by randomly selecting not only the event but also the tidal state when it occurs, and modelling both tsunami and tides together). This approach would, however, significantly increase the number of inundation simulations required in order to get a representative sample.

Methods to include the tides within probabilistic tsunami inundation assessments are still being developed internationally. The current state-of-the-art is to model a representative maximum wave height, assume that the maximum arrival has a period of 20 minutes and that its height falls off exponentially with time. This information can then be used in conjunction with tidal information to sample the probability density function (PDF) of possible inundation depths (Gonzalez et al., 2009; Mofjeld et al., 2007). However, this approach does not include full inundation modelling. By modelling inundation explicitly, extra information about wave arrivals in different areas is obtained.

Figure 13

Time series of the largest (a) and smallest (b) tsunami arriving at point 1 (see Figure 15) and the PDFs of the maximum sea level attained given that the tsunami could arrive at any point in the tidal cycle (c and d respectively).

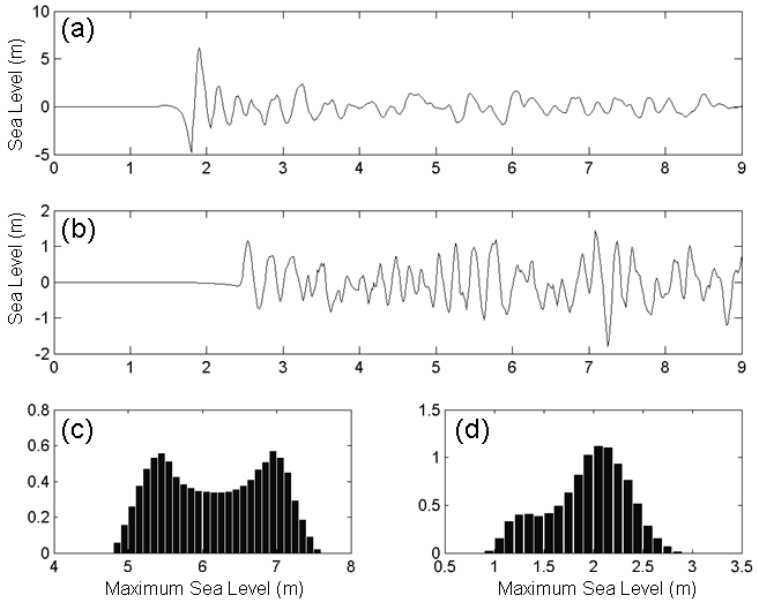

The concept proposed here is to use the time series of water level at each inundation area due to the tsunami together with local tidal information for that area to develop a PDF of maximum sea level. Figure 13 shows two tsunami time series (a) and (b) for a point by the coast at Omaha. By combining each time series with the local tidal time series at different temporal offsets, we can calculate the different possible maximum sea levels and the probability that they will occur. Figure 13 (c) and (d) show this for the two time series. Where there is one large arrival considerably bigger than the rest of the waves (Figure 13a), the PDF is very similar to the tidal PDF plus the maximum wave height. For more complex wave arrivals (Figure 13b), the PDF is similarly more complex (Figure 13d). Figure 14 shows the time series of the 'same' tsunami arriving at different times (offsets) in the tidal cycle, and illustrates how the maximum sea level achieved depends on the time of tsunami arrival relative to the tidal cycle. For example in the case shown, peak water levels occur when the tsunami arrival is offset by about 20 hours and the tsunami coincides with a larger tide. With an offset of about

13 hours, the tsunami arrives at low water and its impact on water level is effectively cancelled.

Lower frequency fluctuations in storm surge and MLoS (monthly to annual variations in the Mean Level of the Sea) are not included in this analysis, but could also further affect the PDF. Because the storm surge and the MLoS occur on sufficiently slow timescales that they do not vary significantly over the tsunami event, these could be taken into account by convolving the maximum sea level PDF with storm surge and MLoS PDF. This is beyond the scope of the present study, however.

Figure 14

Time series of sea level heights during a tsunami as a function of time (hours) and offset against a 12-hour tidal cycle. The blue lines represent time series with 0, 6, 12 and 18 hours offset.

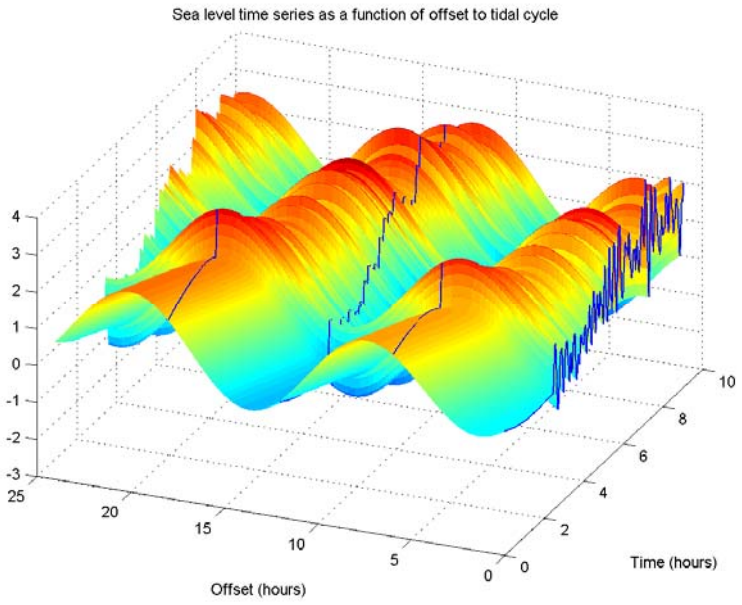

In order to incorporate tidal effects, the tsunami inundation is re-modelled with a baseline set at Highest Astronomical Tide (HAT) rather than MHWS. From this modelling, we determine the inundation from the highest possible water level due to tide and tsunami, rather than that from a tsunami arriving at an "average" high tide. The PDF derived from the tsunami time series and the local tidal series is then used to weight successively reduced levels of inundation until an element is dry. In addition to this, any element which becomes disconnected from the sea as the inundation depths are ramped back has its inundation set to zero, on the assumption that the threshold level needed to inundate this area has not been reached. Again, the inundation over a given threshold h_0 from all the scenarios is summed and those elements whose contribution sum to more than 40 are marked as being inundated by an h_0-level at least once, on average, every 2500 years. The difference from the previous (non-tidal) approach is that, within each scenario, there are different contributions weighted by the PDF.

The probability that a given point x_0 will be inundated to greater than depth h_0 within a given year is then:

$$P(\max_{\text{annual}}(I(x_0)) > h_0) = \frac{1}{L}\sum_{i=1}^{N}\sum_{j=1}^{M} g_{ij}\, d\eta \left[I_{ij}(x_0) > h_0 \right]$$
$$= \frac{1}{L}\sum_{i=1}^{N}\sum_{j=1}^{M} g_{ij}\, d\eta \left[I_i(x_0) > h_0 + (M - j)d\eta \right]$$

where g_{ij} is the probability density of an element being inundated during tsunami event *i* and at tidal state *j*, and $d\eta$ is the step size of the tidal PDF.

Thus the 1:L_0 year exceedance of h_0 inundation area is calculated as before,

$$\left\{ x : P(\max_{\text{annual}}(I(x)) > h_0) \geq \frac{1}{L_0} \right\}.$$

Tsunami and tidal time series were collected for the point locations shown in Figure 15. Tidal time series for inner harbour reaches were derived using a Ports of Auckland co-tidal chart along with tidal constituents taken from analysis of sea level data at Auckland CBD (R.Bell, pers comm, based on data from Ports of Auckland Ltd.). Tidal series for the outer Hauraki Gulf (Orewa etc, Waiheke Island) and Firth of the Thames were derived using constituents from NIWA's harmonic tidal model Tide2D *(Walters et al., 2001, Walters, 2005)*.

3.5 Mapping and Presentation of Results

In this report, the phrase "inundation depth" refers to the depth of water that flows onto land above MHWS as a result of the tsunami. At any location, it is equivalent to the tsunami run-up height (relative to mean sea level) minus the elevation of the land above mean sea level at that location.

Figure 15

Point locations where time series were taken for PTHA including tides. Tidal data at locations denoted by red squares were used to analyse inundation in 'central' Auckland areas; data from sites denoted by blue triangles were used for 'distal' Auckland inundation areas (see text for more details).

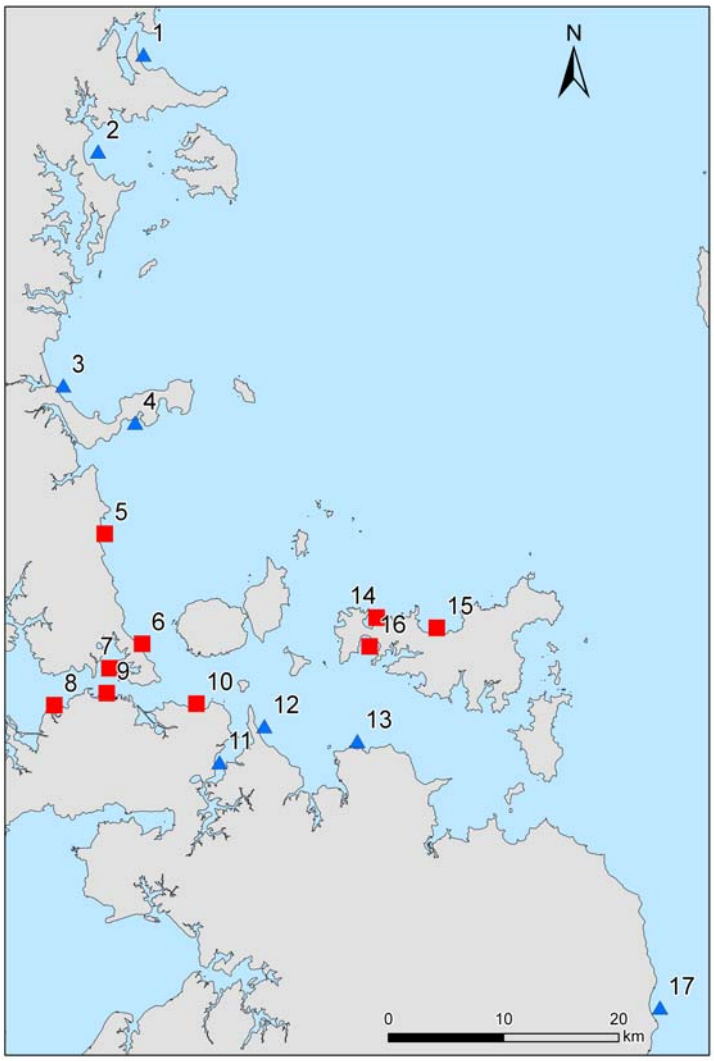

Results are produced for the seven areas for which inundation modelling were carried out in Lane, et al. (2007). These areas are:

- Omaha, Snells Beach to Martins Bay;
- Waiwera to Whangaparaoa Peninsula;
- Browns Bay to Devonport;
- Te Atatu to St Heliers, including CBD;
- Panmure to Maraetai;

- Waiheke Island (Oneroa, Surfdale, Onetangi);
- Kaiaua.

For each of the land areas, probabilistic inundation at the 2500-year ARI for depths of 0.1, 0.5, 1, 1.5, 2 and 2.5 m are shown. These should be understood as illustrating the area predicted to be inundated to at least that depth at least once every 2500 years, on average, over a long (e.g. 100 000 years) period of time. Two versions of each map are shown: the first version shows predicted inundation if all tsunami occur at MHWS; the second version shows predicted inundation if variation in tidal height is taken into account during the probabilistic calculations. Because this is a probabilistic study, there is no one particular tsunami event that necessarily inundates to this level everywhere in the model domain. The maps represent an amalgamation of the results from the 100 model tsunami simulations performed. As well as the probabilistic inundation, probabilistic maximum speed maps are also given, in this case for not only the land but the surrounding sea. Again, these represent an amalgamation of the results from the 100 model tsunami simulations, but do not include tidal effects.

4 Results

4.1 Probabilistic Regional Wave Heights

Figures 16 and 17 show the 2500-year probabilistic exceedance levels for wave height (relative to mean sea level) and maximum speed for the east coast of the Auckland region from regional tsunami. As can be readily seen, the east coast of Great Barrier Island bears the brunt of the inundation with probabilistic wave heights of up to 10 m. Pakiri, Omaha, Tawharanui Peninsula and Kawau Island are also reasonably exposed to regional tsunami. Areas further up the Hauraki Gulf are more sheltered, although wave heights of over 2 metres can still be expected at least once every 2500 years for much of the area from Snell's Beach through to Takapuna and the outer sides of Rangitoto, Motutapu and Waiheke islands. The tsunami modelled in the Monte Carlo simulations do not appear to excite significant resonances in the Waitemata Harbour, the Firth of the Thames or any other more inland areas, and the probabilistic hazard from regional tsunami in these areas is relatively low. Likewise the maximum speeds expected from regional tsunami are highest in the more exposed areas and in some of the channels between islands, but are low further up the harbour and in Firth of the Thames.

Figure 16
2500-year ARI exceedance levels for wave heights (metres above mean sea level) due to regional tsunami for the Auckland region.

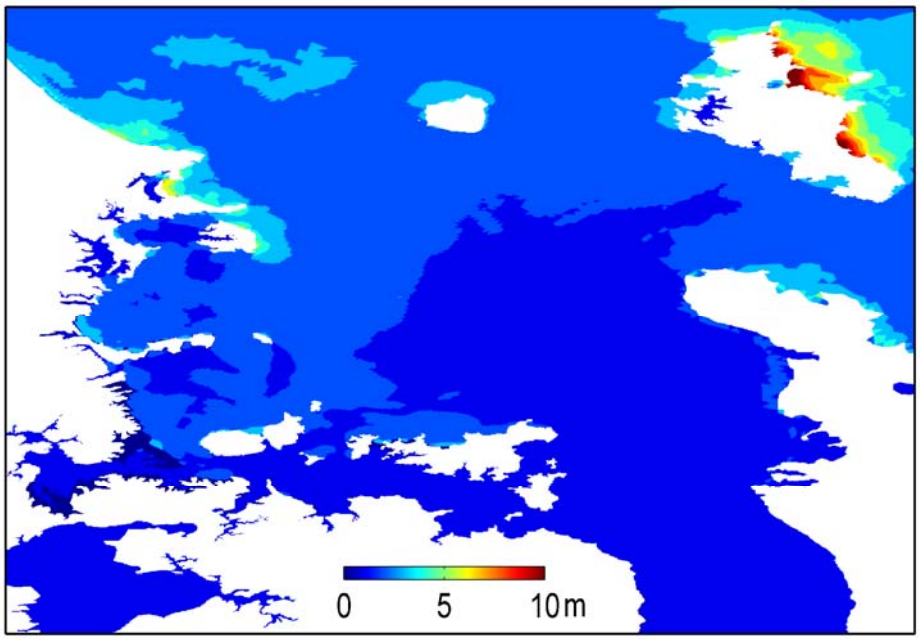

Figure 17
2500-year ARI exceedance levels for maximum speed (m s^{-1}) due to regional tsunami for the Auckland region.

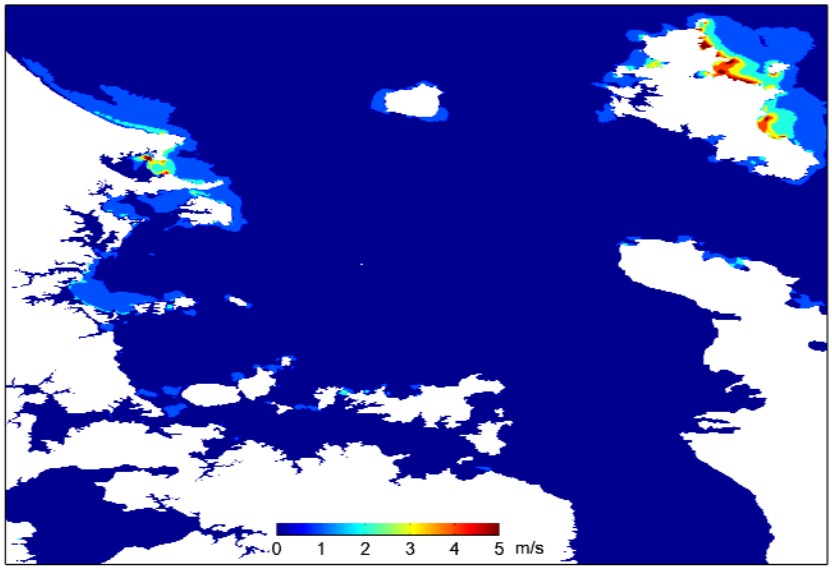

The maximum predicted wave heights for each coastal location shown in Figure 15 from all 100 modelled tsunami events are tabulated in Appendix 2. The wave heights are given relative to mean sea level, and do not include the MHWS elevation of 1.4 m.

4.2 Probabilistic Tsunami Hazard Assessment: Omaha and Snells Beach to Martins Bay

The 2500-year ARI probabilistic inundation for Omaha to Martins Bay is shown in Figures 18 and 19. The 2500-year ARI probabilistic maximum speed is shown in Figure 20. Much of the seaward side of Omaha peninsula will be inundated at least once on average, every 2500 years, including a considerable part of the built up area. Whangateau, on the north of the Harbour is also inundated as well as inner Whangateau Harbour areas. The shoreline of Snell's Beach, Algies Bay and Martin's Bay are also inundated to around 100 m inland. When the tides are included in the PTHA rather than the modelling being done at MHWS (Figure 19) this inundation is generally not as extensive, especially in the inner Harbour areas. There is still considerable inundation on the seaward side of the peninsula, at Whangateau and Snell's Beach, Algies Bay and Martin's Bay, but it is not as deep. Figure 20 shows the maximum speeds. These are high (greater than 2 m s^{-1}) for the seaward side of Omaha and the entrance to the harbour, gradually decreasing at the upper ends of the harbour. They are lower for Snell's Beach, Algies Bay and Martin's Bay which are sheltered by Tawharanui Peninsula and Kawau Island but they still reach over 2 m s^{-1} around headlands, at the entrance to Matakana River and the run off from Martin's Bay.

Figure 18

2500-year ARI exceedances for regional probabilistic tsunami inundation at MHWS: Omaha and Snells beach to Martins Bay.

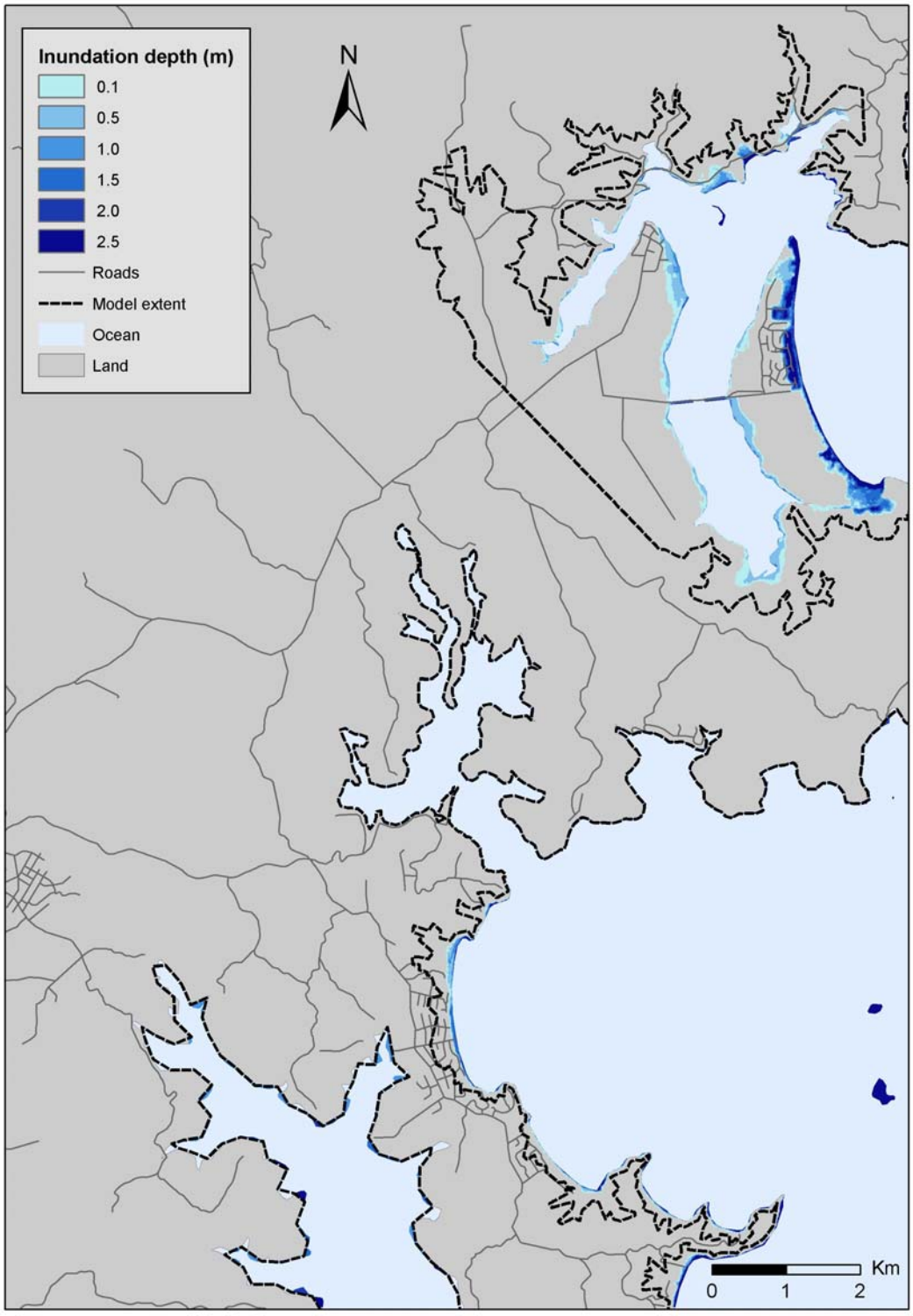

Figure 19

2500-year ARI exceedances for regional probabilistic tsunami inundation including tidal effects: Omaha and Snells beach to Martins Bay.

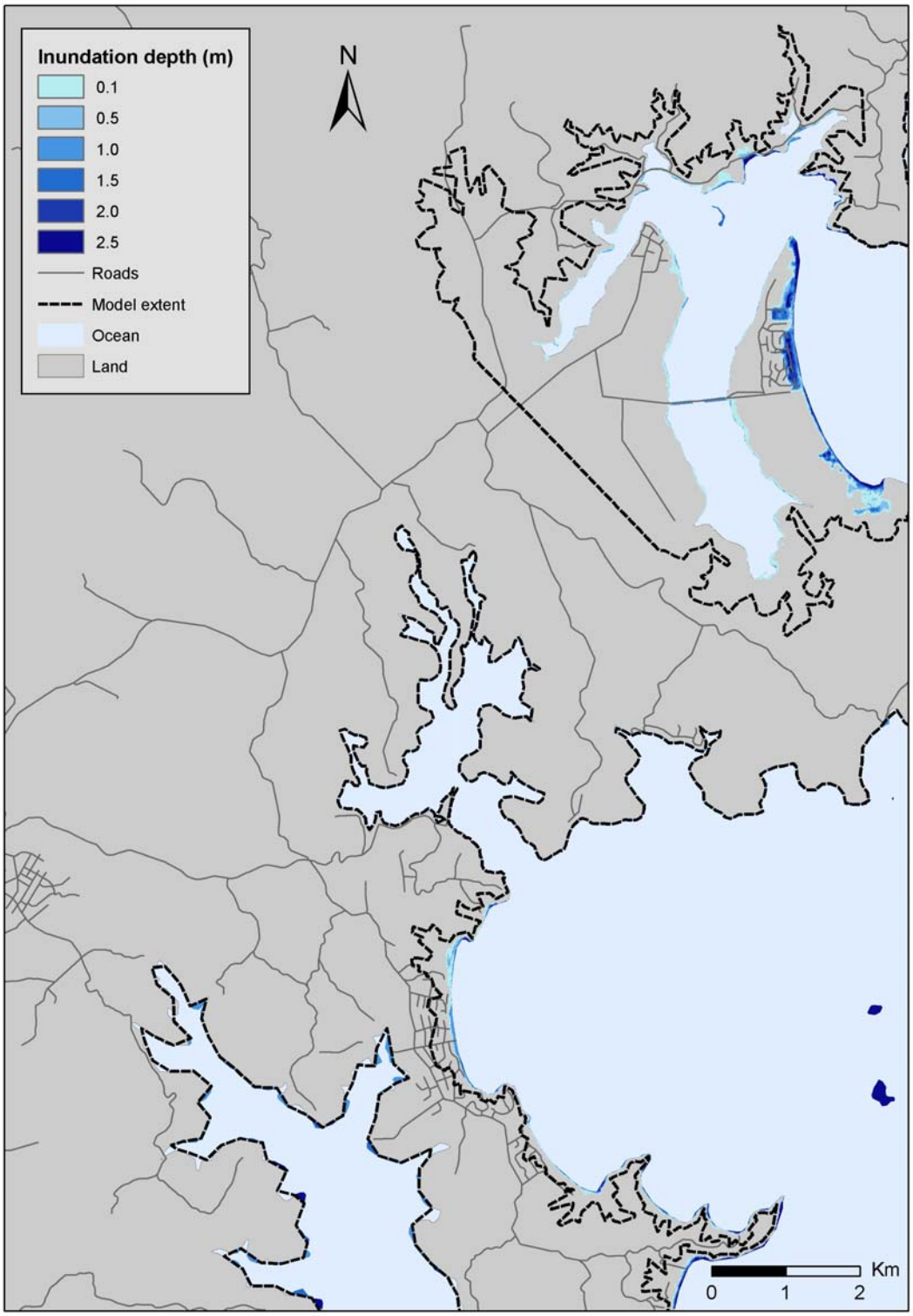

Figure 20

2500-year ARI exceedances of maximum speed for probabilistic tsunami hazard: Omaha and Snells Beach to Martins Bay.

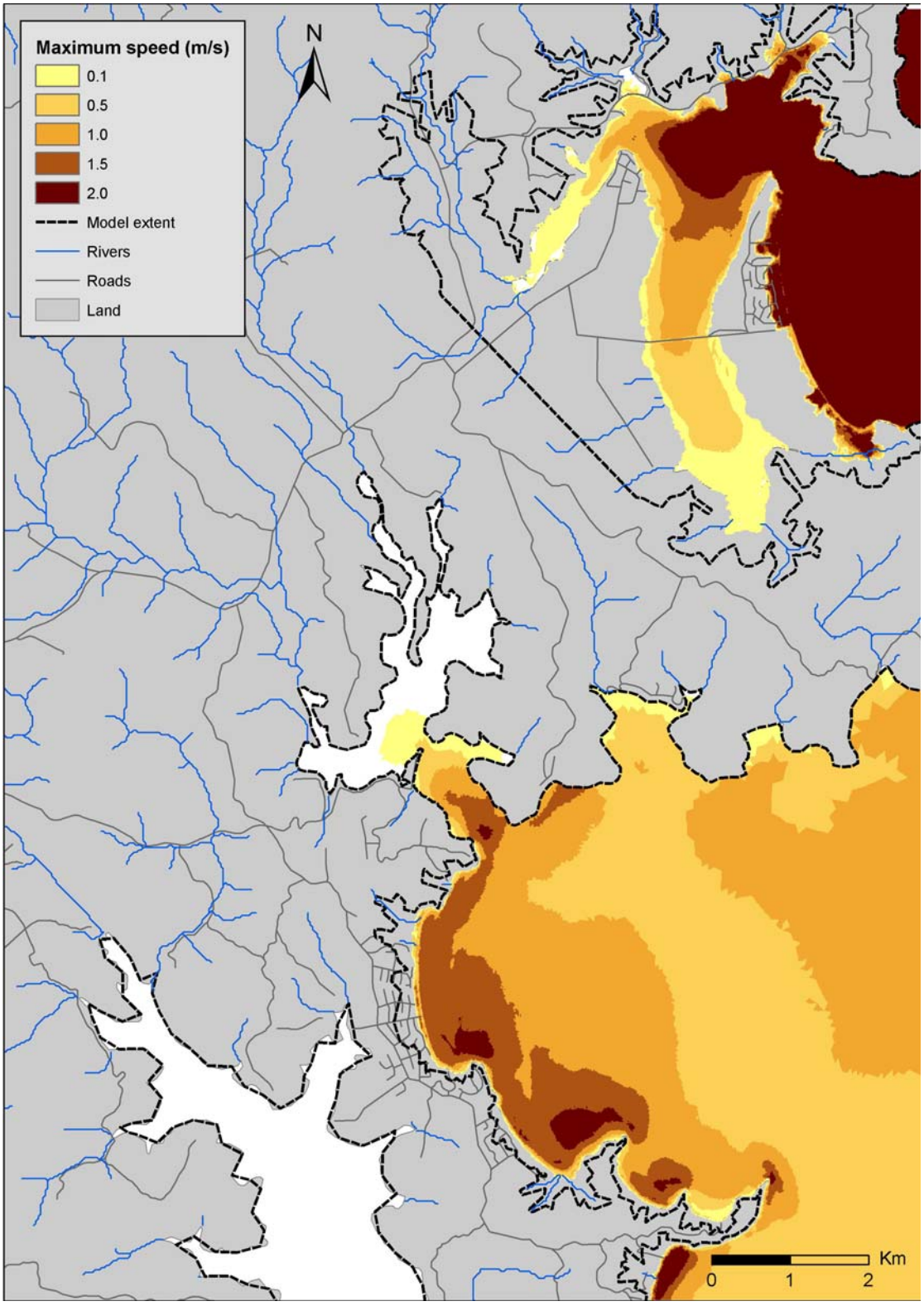

4.3 Probabilistic Tsunami Hazard Assessment: Waiwera to Whangaparaoa Peninsula.

Figures 21 and 22 show the probabilistic tsunami inundation from regional tsunami in the areas from Waiwera to Whangaparaoa modelled at MHWS and including tidal heights respectively. Inundation of state Highway 1 is seen North of Hatfield Beach as well as the Camp ground at Orewa, the southern end of Stanmore Bay and Okoromai Bay and Hobbs Bay on the southern side of Whangaparaoa Peninsula. The beach and nearshore region of other areas is also inundated up to about 100 m inland in many places. For the MHWS models, the inundation of SH1 north of Hatfield Beach and the camp ground at Orewa is much more severe than with the full tidal effects. Also, for the modelling at MHWS, the Orewa oxidation ponds are inundated at the 2500-year ARI exceedance, whereas when the full tidal effects are taken into account this inundation does not occur. Maximum speeds (as shown in Figure 23) are high all along Orewa Bay and Stanmore Bay, the heads along Whangaparaoa Peninsula and in Okoromai Bay, but tend to be slightly lower further south than this.

Figure 21
2500 year exceedances for regional probabilistic tsunami inundation at MHWS: Waiwera to Whangaparaoa Peninsula.

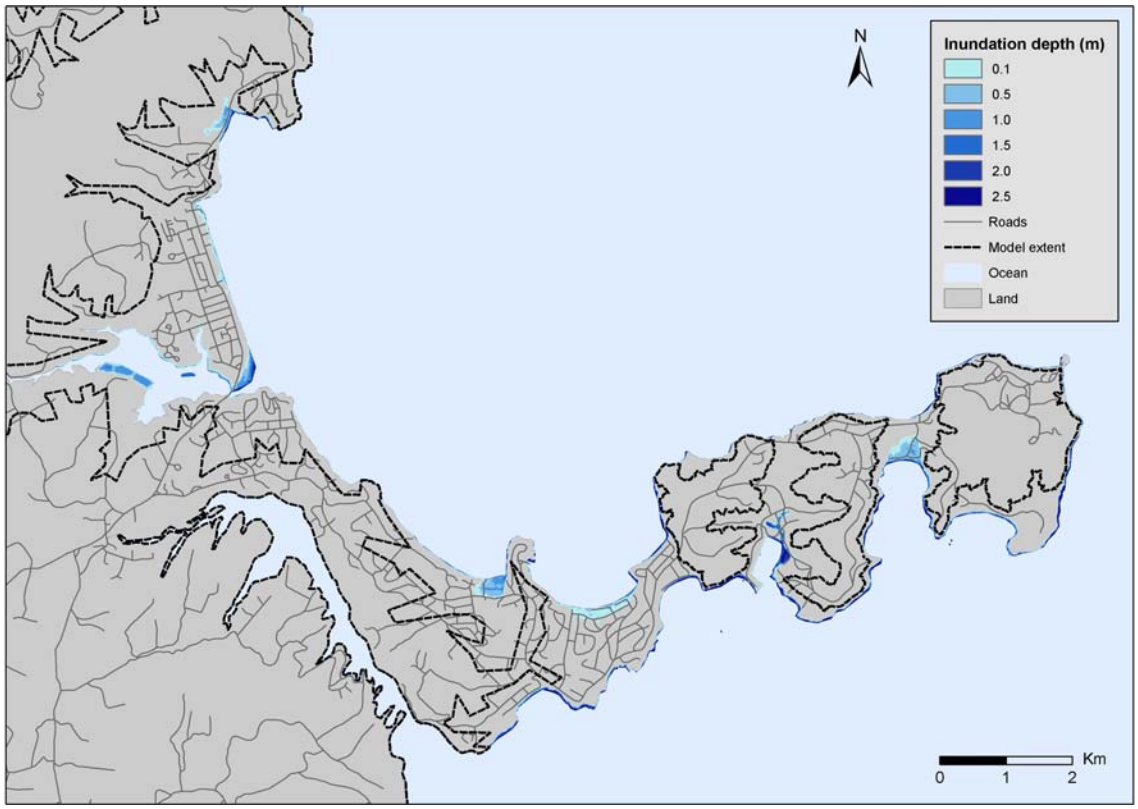

Figure 22

2500-year ARI exceedances for regional probabilistic tsunami inundation including tidal effects: Waiwera to Whangaparaoa Peninsula.

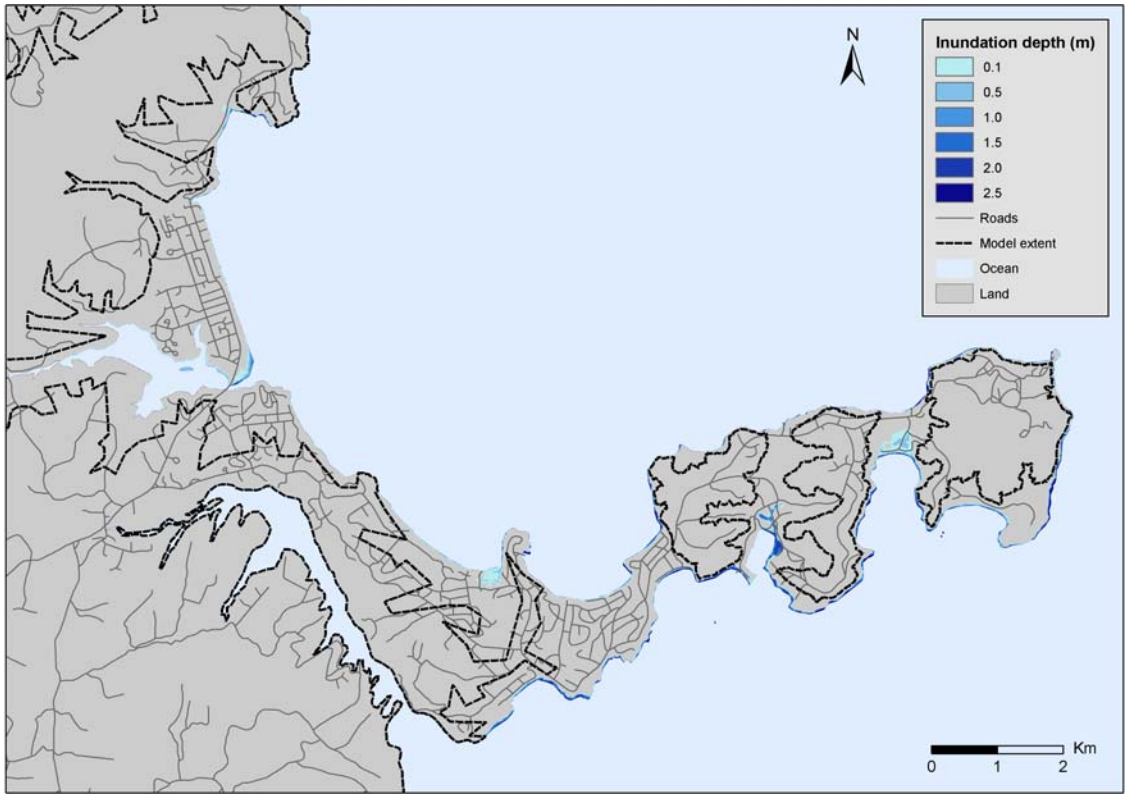

Figure 23

2500-year ARI exceedances of maximum speed for probabilistic tsunami hazard: Waiwera to Whangaparaoa Peninsula.

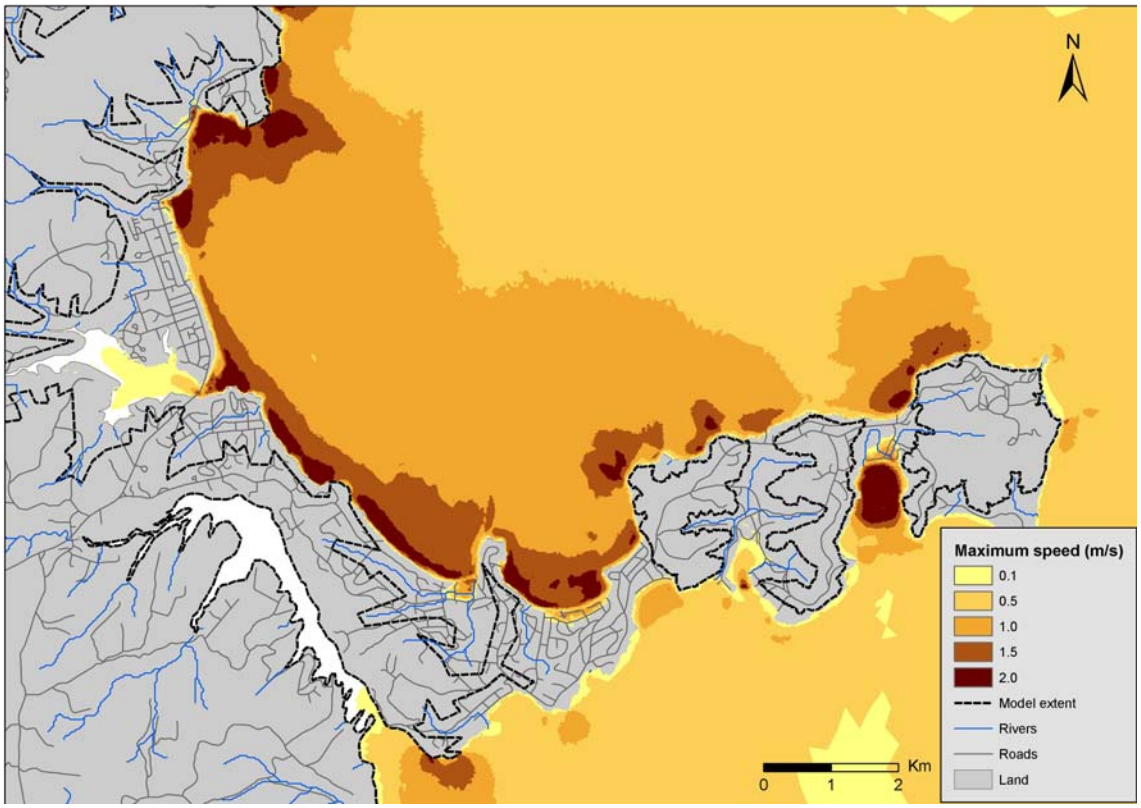

4.4 Probabilistic Tsunami Hazard Assessment: Long Bay to Devonport and Northcote.

The 2500-year ARI probabilistic inundation for Long Bay to Devonport and Northcote is shown in Figures 24 and 25. The 2500-year ARI probabilistic maximum speed is shown in Figure 26. A considerable amount of the coastline is inundated up to 100 – 200 m inland in this area, especially Browns Bay, Mairangi Bay and Milford although only small amounts of this inundation are over roads. Devonport and SH1 at Northcote are exposed to inundation that reaches close to, and over in places, the waterfront roads. The dry dock at the naval base in Devonport is inundated. Including tidal effects does not generate significant differences from the predicted inundation patterns at MHWS. This may be due to the fact that the topography in much of this region is steep with only a small amount of low-lying land near the sea. Those areas with the lowest lying land tend to be found within Waitemata Harbour where the effects of regional tsunami are less extreme. Maximum speeds are highest around headlands but only exceed 1.5 m s^{-1} in localised regions.

Figure 24

2500-year ARI exceedances for regional probabilistic tsunami inundation at MHWS: Long Bay to Devonport and Northcote.

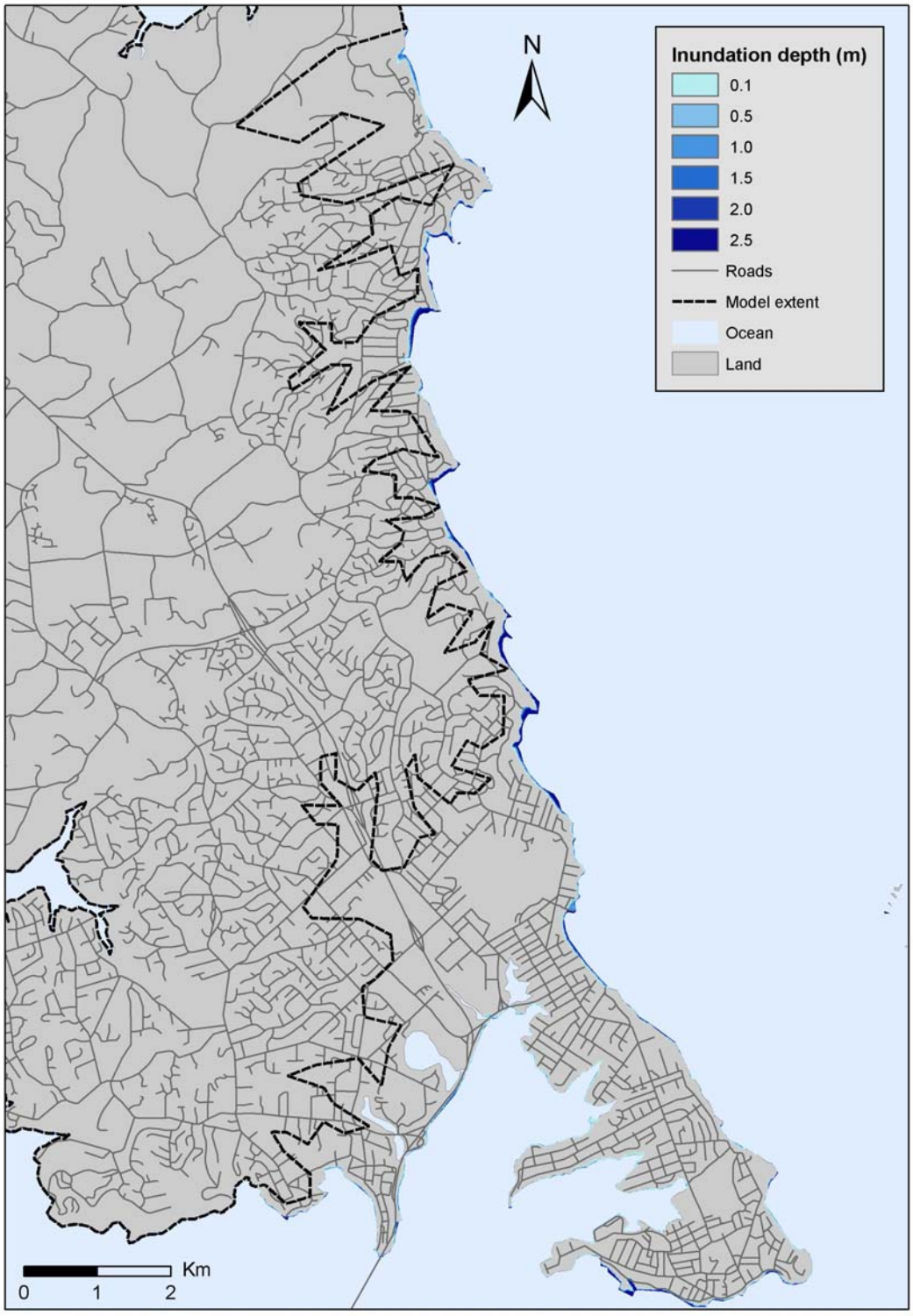

Figure 25

2500-year ARI exceedances for regional probabilistic tsunami inundation including tidal effects: Long Bay to Devonport and Northcote.

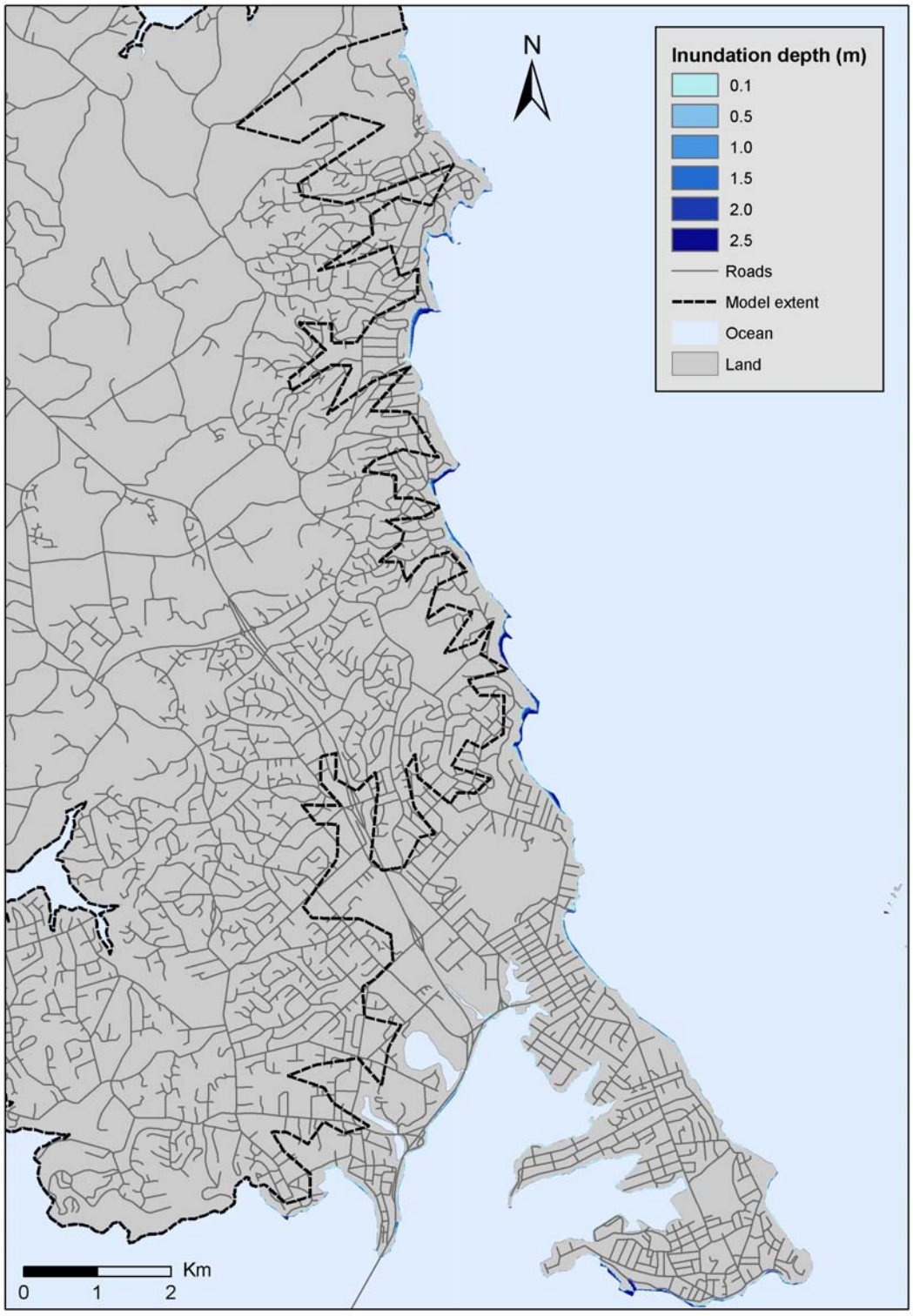

Figure 26

2500-year ARI exceedances of maximum speed for probabilistic tsunami hazard: Long Bay to Devonport and Northcote.

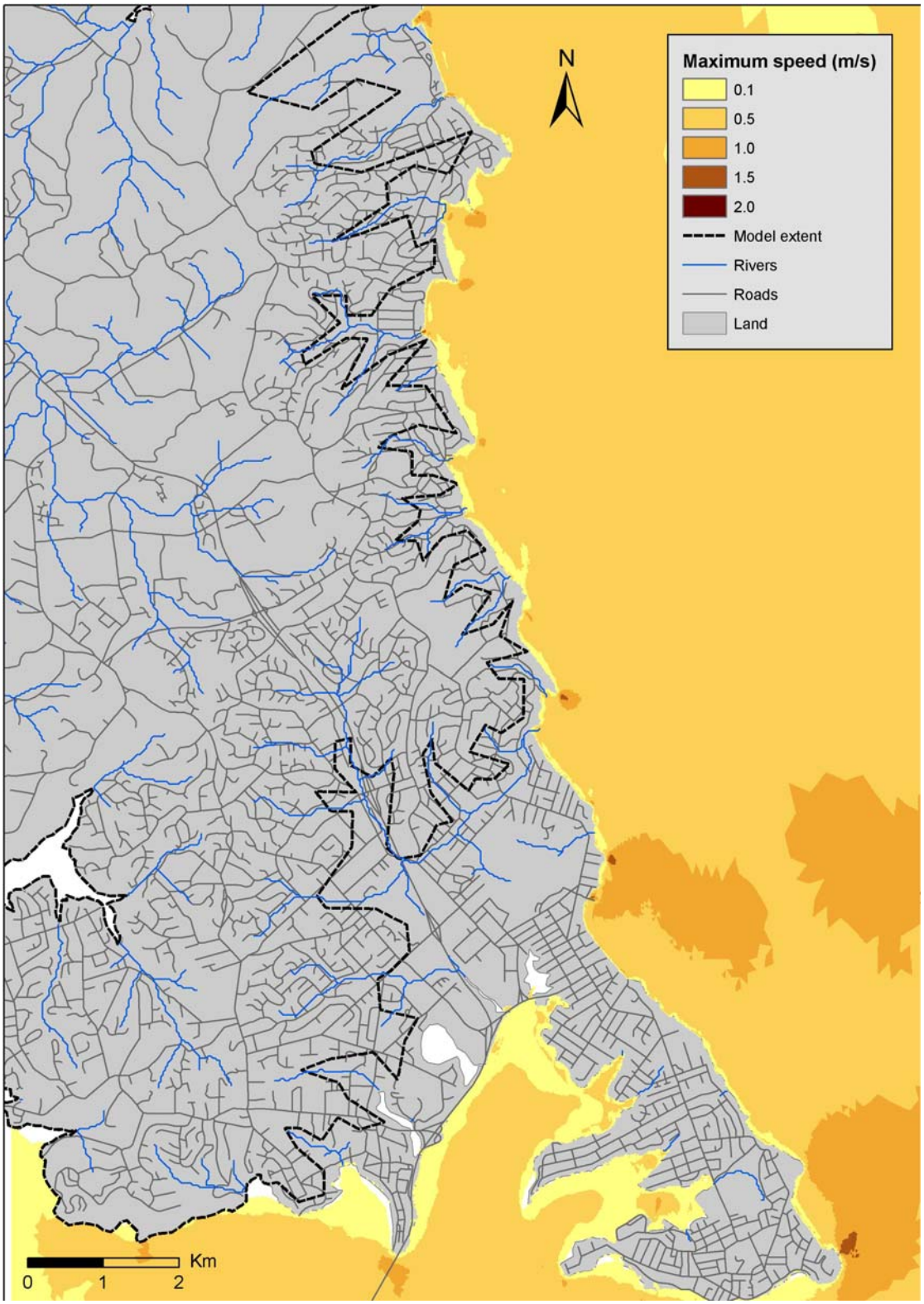

4.5 Probabilistic Tsunami Hazard Assessment: Te Atatu to St Heliers, including CBD.

The 2500-year ARI probabilistic inundation for Te Atatu to St Heliers, including the CBD is shown in Figures 27 and 28. The 2500-year ARI probabilistic maximum speed is shown in Figure 29. This area is well protected from tsunami inundation by its position behind not only Great Barrier Island but also Rangitoto and Motutapu Islands. Because of this, regional tsunami do not strongly impact this area. The modelling predicts most of the inundation due to tsunami at the 2500-year exceedance level in this area is confined to the coastline. The inundation of Pollen Island shown is a result of poor resolution in the model rather than expected inundation. Most inundation is seen at Westhaven Marina. The NW motorway between Point Chevalier and Te Atatu and Tamaki Drive at Hobsons Bay are at risk of inundation. Maximum speeds are generally not high. They are greatest around headlands.

Figure 27
2500-year ARI exceedances for regional probabilistic tsunami inundation at MHWS: Te Atatu to St Heliers, including CBD.

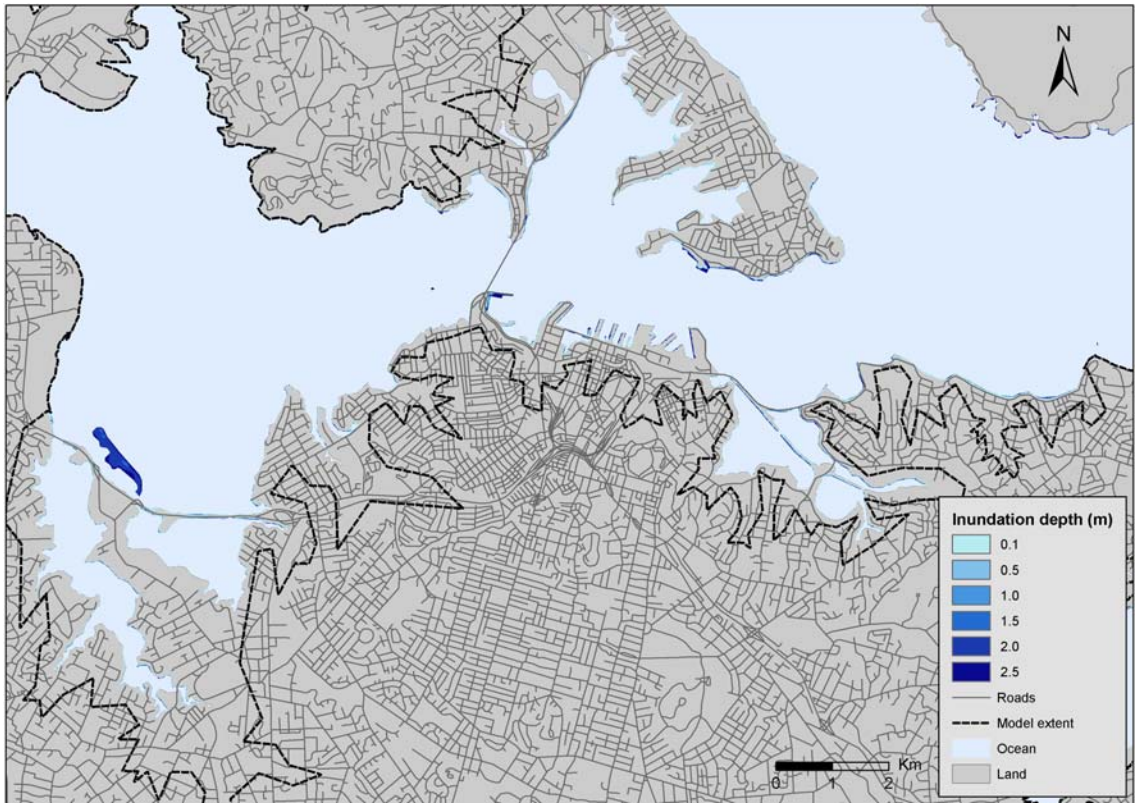

Figure 28

2500-year ARI exceedances for regional probabilistic tsunami inundation including tidal effects: Te Atatu to St Heliers, including CBD.

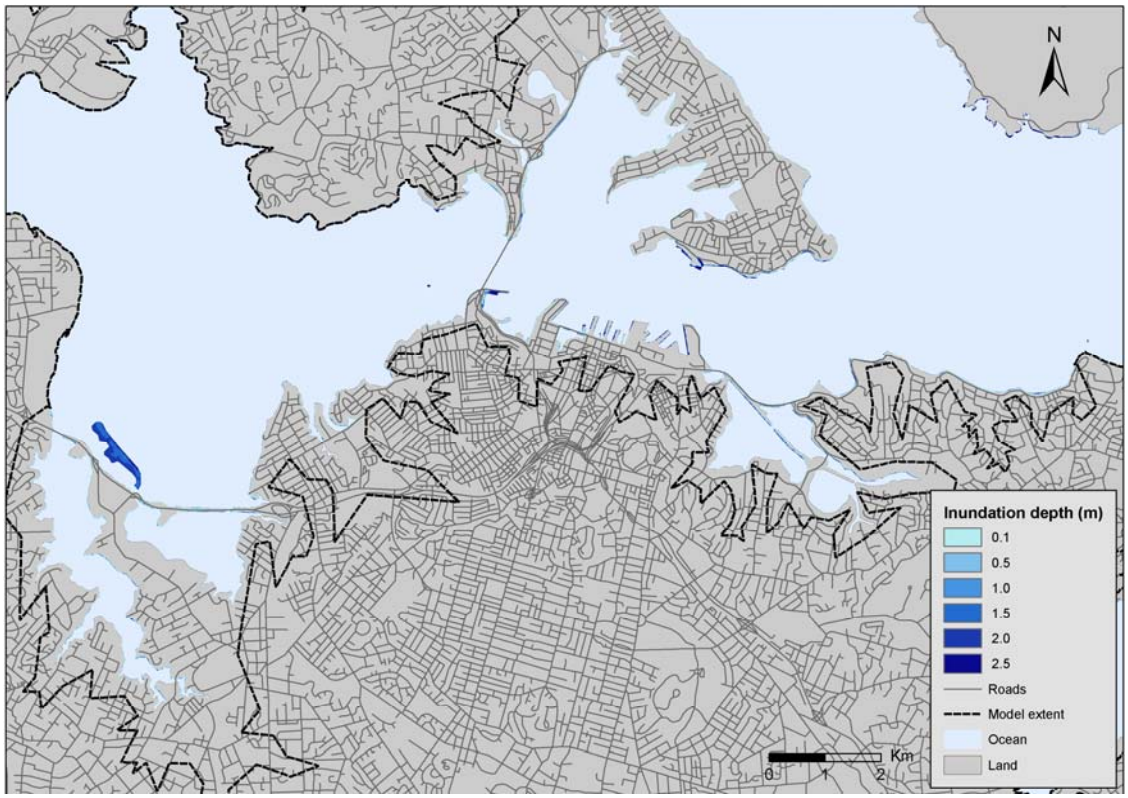

Figure 29

2500-year ARI exceedances of maximum speed for probabilistic tsunami hazard: Te Atatu to St Heliers, including CBD.

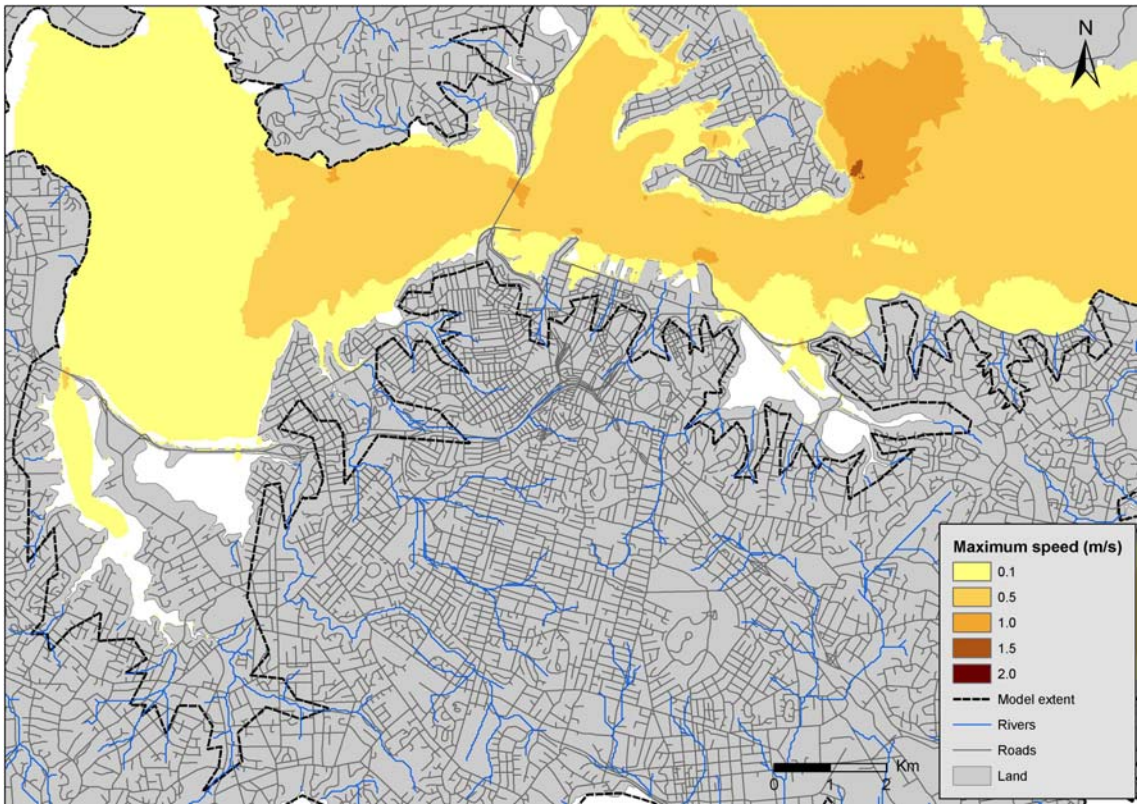

4.6 Probabilistic Tsunami Hazard Assessment: Panmure to Maraetai.

The 2500-year ARI probabilistic inundation for Panmure to Maraetai is shown in Figures 30 and 31. The 2500-year ARI probabilistic maximum speed is shown in Figure 32. This area is largely protected from regional tsunami inundation by Great Barrier Island and then Rangitoto, Motutapu and Waiheke Islands. Inundation is mostly confined to the beaches. Inundation is the most at Tahuna Torea, Bucklands Beach and the marina at Beachlands. Maximum speeds are highest in the Panmure Inlet but not exceptionally high anywhere.

Figure 30

2500-year ARI exceedances for regional probabilistic tsunami inundation at MHWS: Panmure to Maraetai.

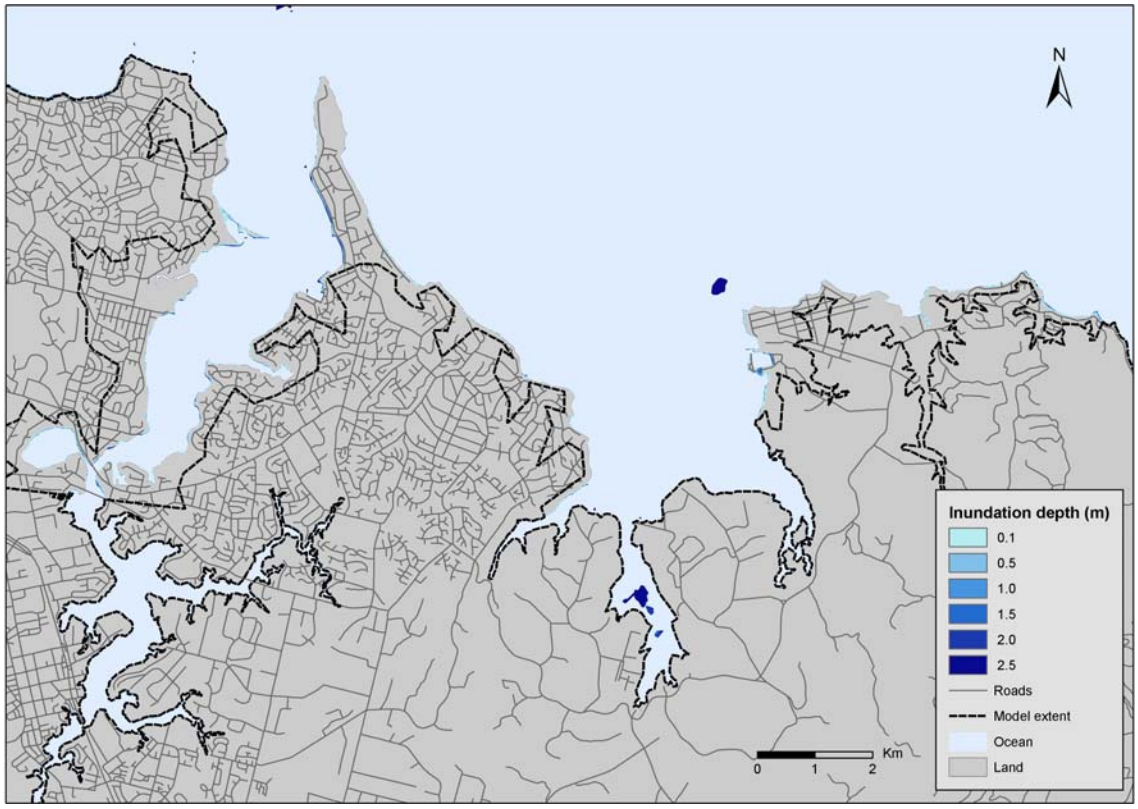

Figure 31

2500-year ARI exceedances for regional probabilistic tsunami inundation including tidal effects: Panmure to Maraetai.

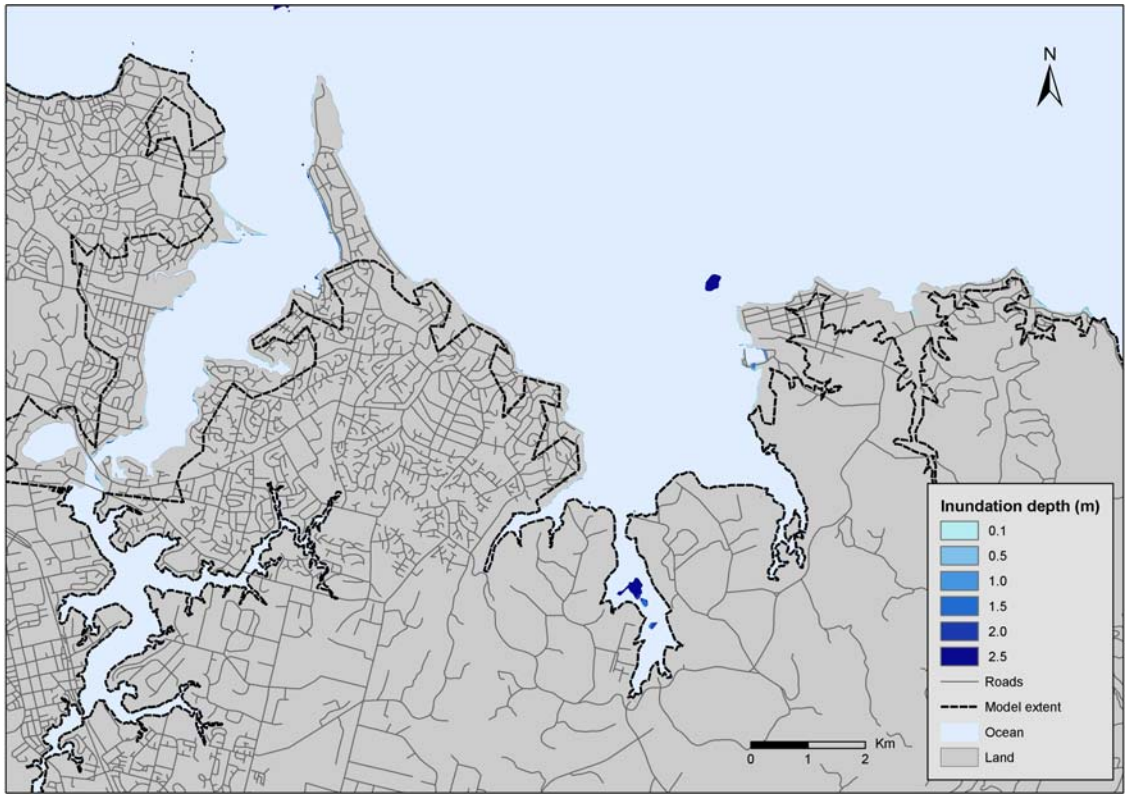

Figure 32

2500-year ARI exceedances of maximum speed for probabilistic tsunami hazard: Panmure to Maraetai.

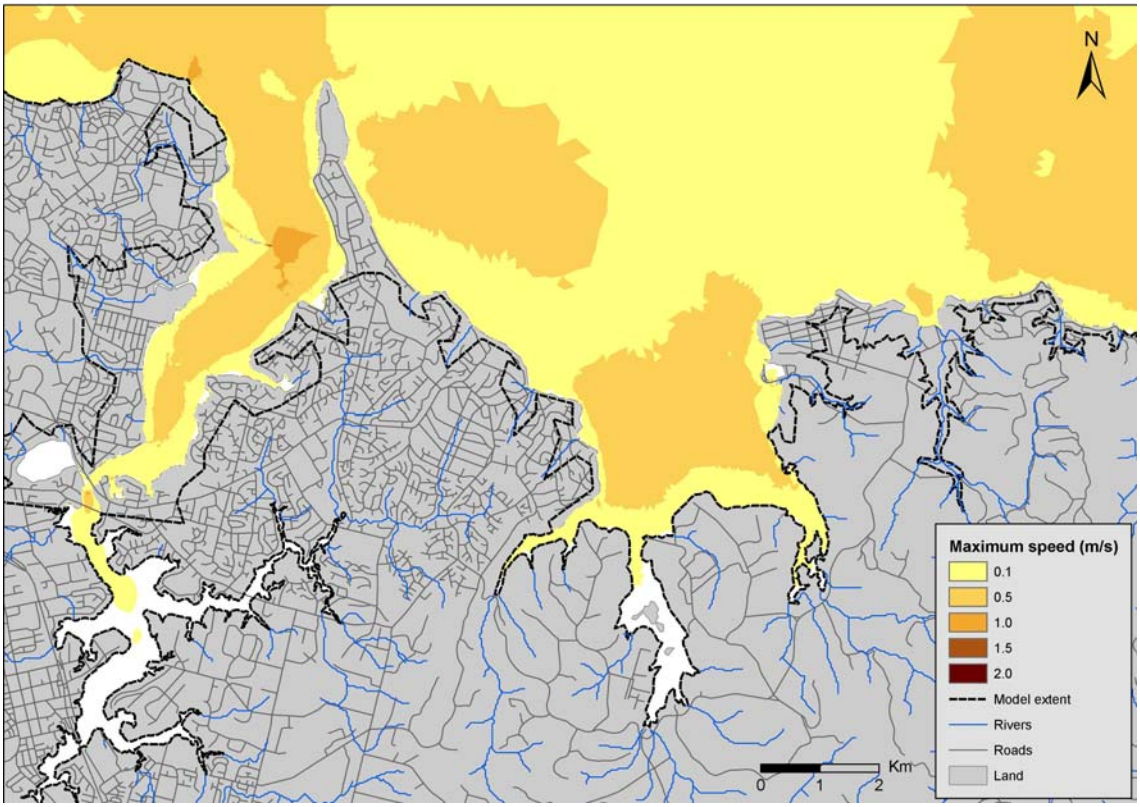

4.7 Probabilistic Tsunami Hazard Assessment: Waiheke Island.

The 2500-year ARI probabilistic inundation for Waiheke Island is shown in Figures 33 and 34. The 2500-year ARI probabilistic maximum speed is shown in Figure 35. The inundation of Waiheke Island is also confined mainly to the coastal strip. Most of the beach at Onetangi is inundated with water reaching the road at the eastern end. Several little bays on the northern side are inundated quite deeply. Blackpool and Surfdale are also inundated over the coastal roads in places, but generally not as deeply as the northern side of the island. When tides are included in the analysis, these effects are not as profound. Maximum speeds are highest in Oneroa and Mawhitipana Bays.

Figure 33

2500-year ARI exceedances for regional probabilistic tsunami inundation at MHWS: Waiheke Island.

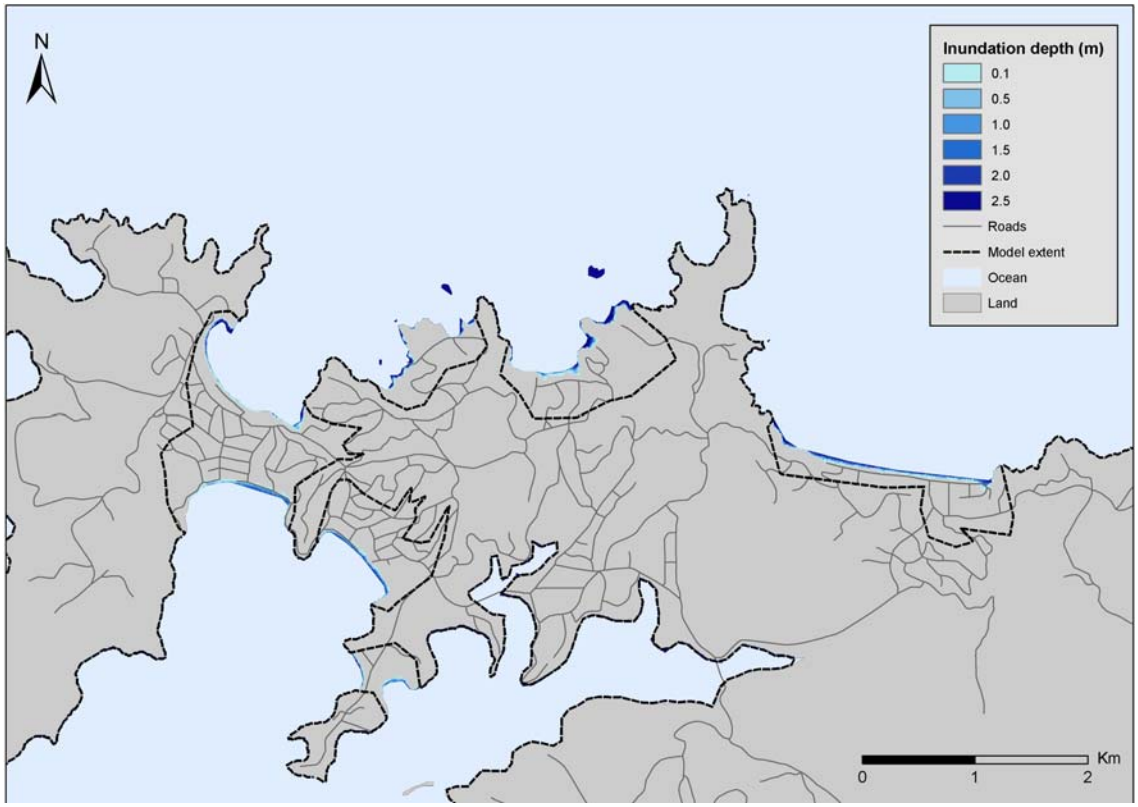

Figure 34

2500-year ARI exceedances for regional probabilistic tsunami inundation including tidal effects: Waiheke Island.

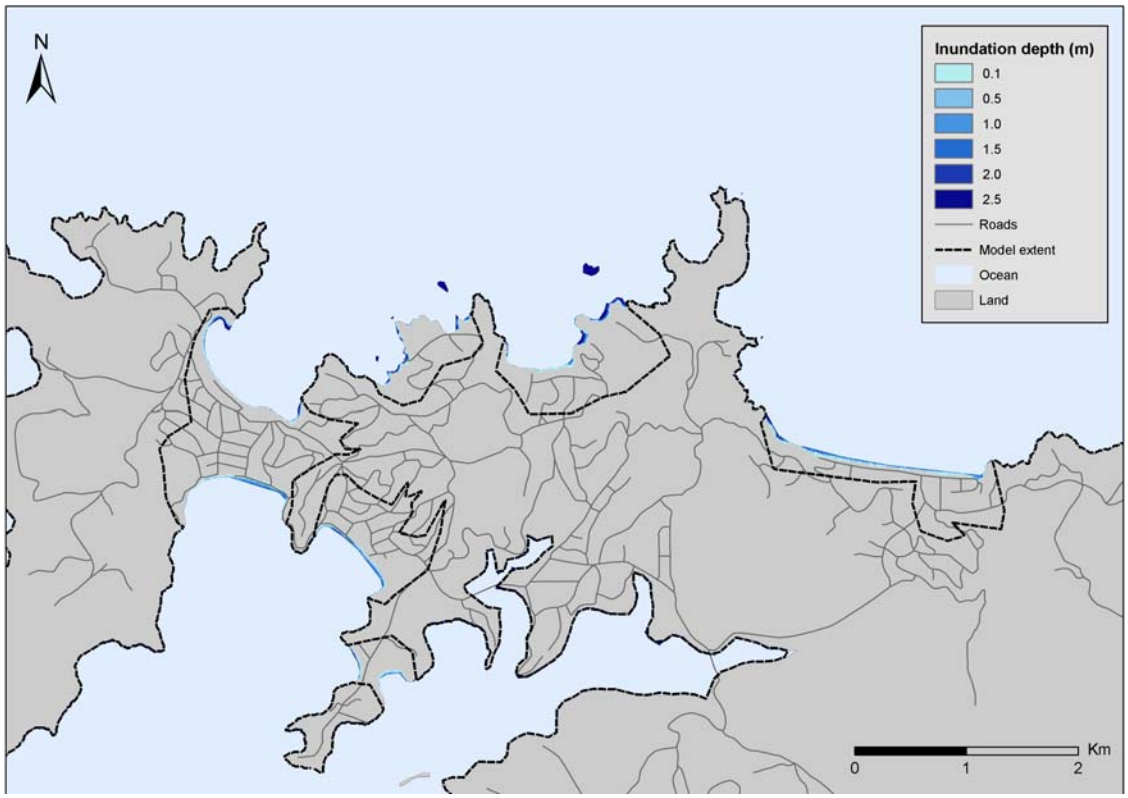

Figure 35
2500-year ARI exceedances of maximum speed for probabilistic tsunami hazard: Waiheke Island.

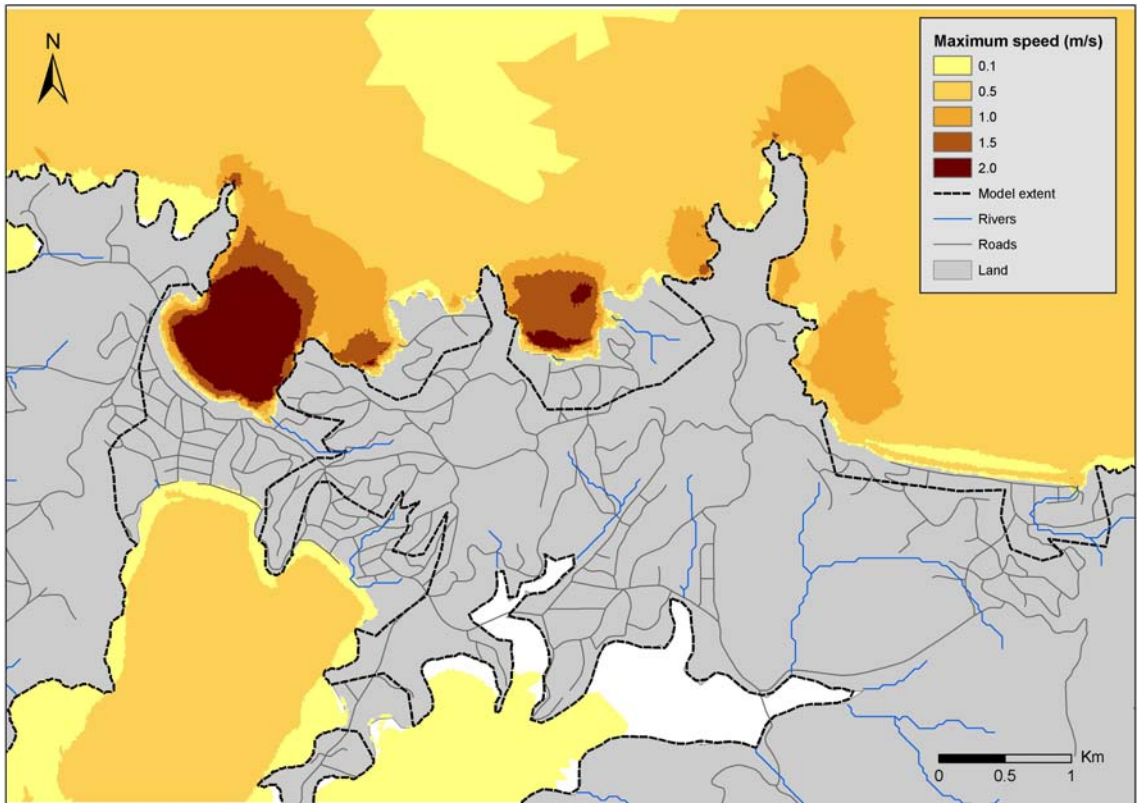

4.8 Probabilistic Tsunami Hazard Assessment: Kaiaua.

The 2500-year ARI probabilistic inundation for Kaiaua is shown in Figures 36 and 37. The 2500-year ARI probabilistic maximum speed is shown in Figure 38. While there is a small amount of shallow inundation near the coast for Kaiaua in the regional probabilistic tsunami hazard assessment this appears to be fairly minor. Maximum speeds are not high.

Figure 36

2500-year ARI exceedances for regional probabilistic tsunami inundation at MHWS: Kaiaua.

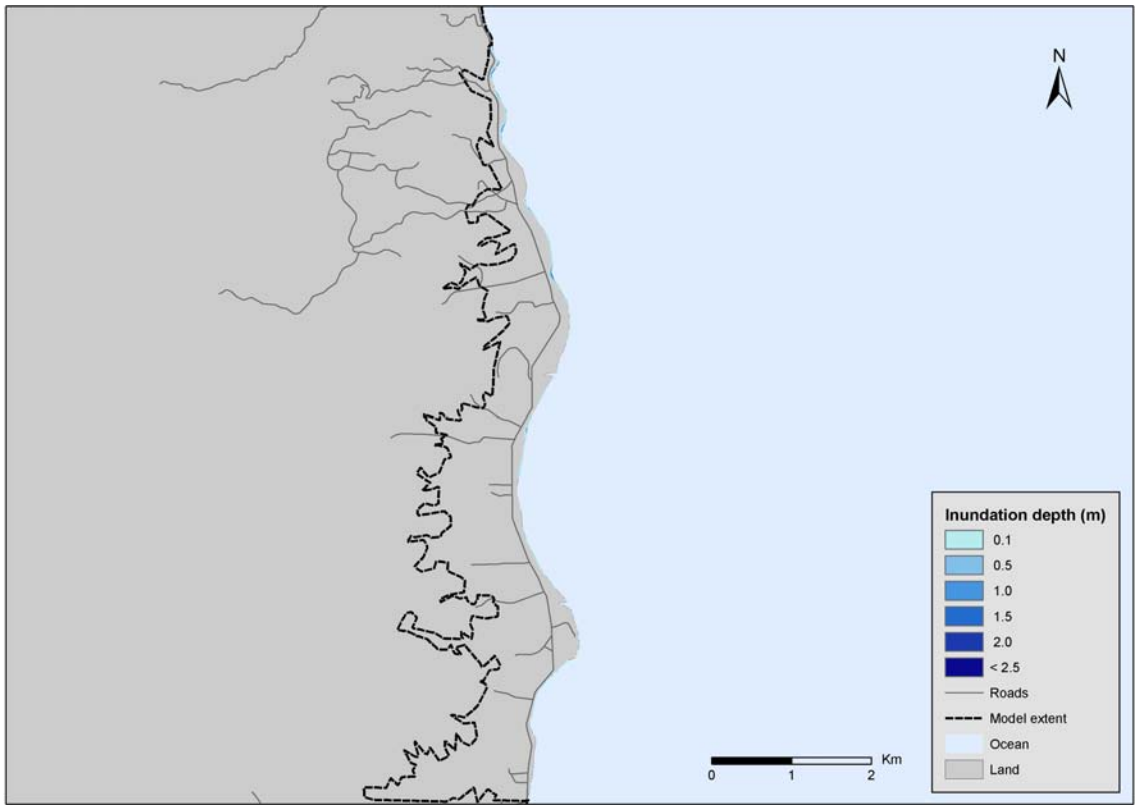

Figure 37

2500-year ARI exceedances for regional probabilistic tsunami inundation including tidal effects: Kaiaua.

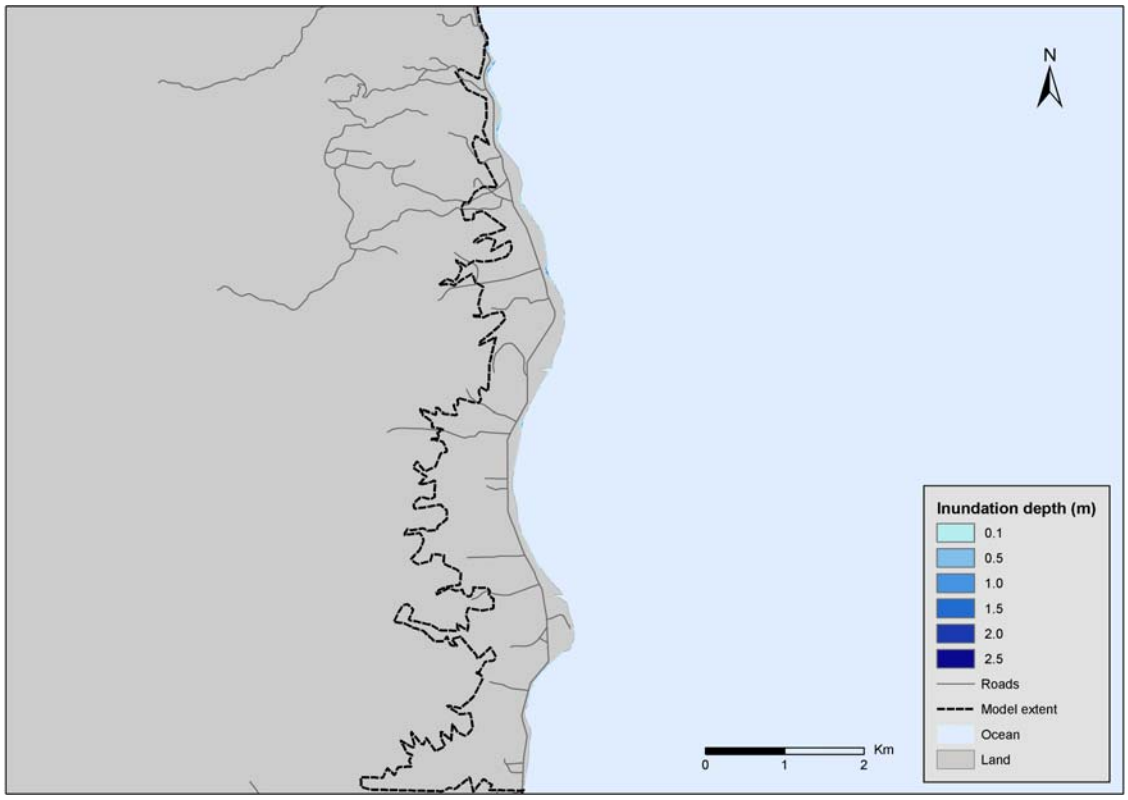

Figure 38

2500-year ARI exceedances of maximum speed for probabilistic tsunami hazard: Kaiaua.

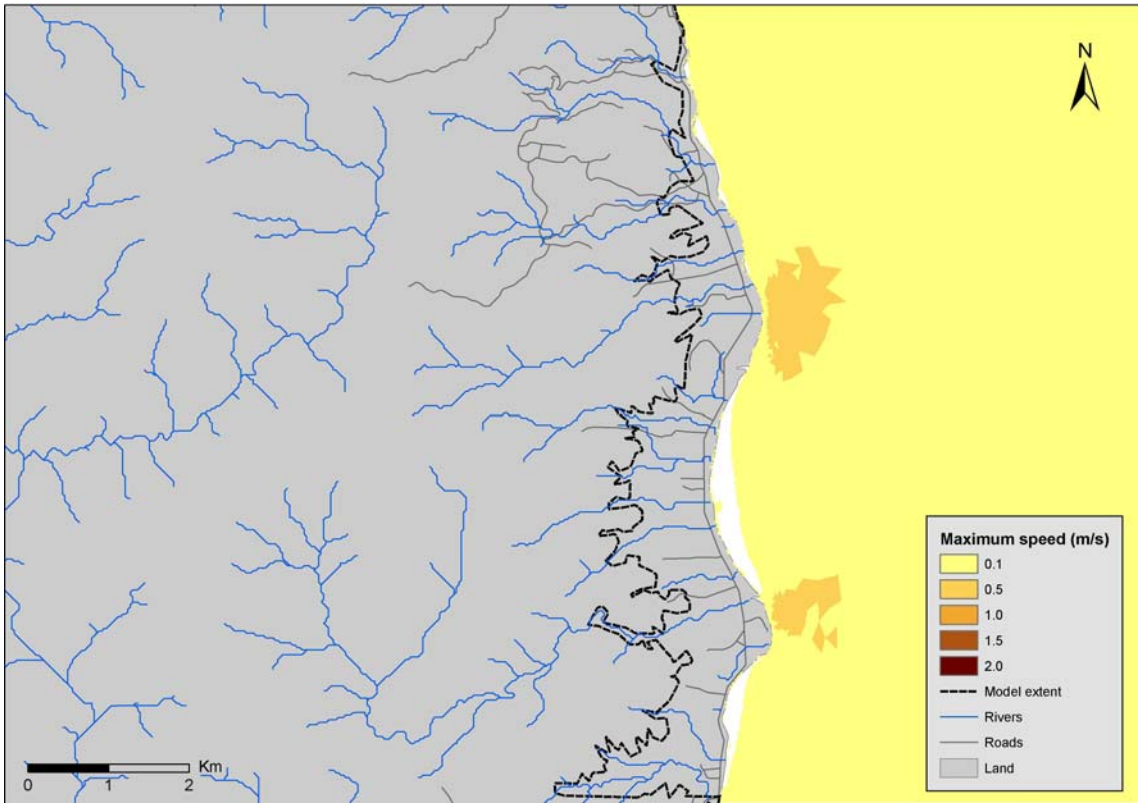

5 Discussion

Tsunami generated by subduction zone earthquakes on the Tonga-Kermadec Arc have the greatest impact on Great Barrier Island, Omaha, Kawau Island and surrounds within the Auckland region. The largest impact is on the east coast of Great Barrier Island where probabilistic wave heights are up to 10 metres in places. Areas further into the Hauraki Gulf are sheltered by these outer islands and the impact of the tsunami there is fairly small. The shorter wavelengths of the regional source tsunami, compared to those of South American origin, reduce the distance that the tsunami propagate up harbours, and there are only small predicted impacts by the tsunami in the upper Waitemata Harbour. Likewise, the probabilistic maximum speeds are also far larger on more exposed aspects than in the inner harbour and Firth of the Thames, where they are generally negligible. Maximum speeds are highest around headlands and in narrow channels where the water is accelerated. Often, maximum current speeds are attained during withdrawal of the tsunami in shallow areas.

5.1 Limitations of Uncertainty Modelling

The uncertainties in the parameters that determine the magnitude-frequency distribution of the tsunami source have been estimated in the logic trees described in Section 2.1, and the influence of the tide on the inundation pattern has also been statistically estimated. However it should be noted that some other causes of uncertainty have not been incorporated: in particular, the source scenarios assume a uniform distribution of slip on the rupture surface. Geist (2002) demonstrated that for a fixed seismic moment, variations in the distribution of slip could affect the peak nearshore tsunami amplitude in the near-field by approximately a factor of about 3. The influence of slip non-uniformity recedes with distance, and in the far field becomes relatively unimportant. In this study, the Kermadec Arc source is in between the near-field and far-field cases, as the distance from the study area to the source region is comparable to the typical rupture lengths of our scenario earthquakes (and is a few multiples of the rupture width). Consequently, the use of a uniform slip distribution must still be regarded as a noteworthy assumption, as the effects of non-uniform slip could potentially raise the estimated hazard level if they were incorporated into the analysis; further scientific research is needed to quantify the effect of non-uniform slip in intermediate-range situations such as this.

Another area of uncertainty not explicitly considered is the uncertainty in the bathymetric mesh, since small scale variations in near-shore bathymetry could play a significant role in determining the peak nearshore tsunami amplitude over small distances.

The logic-tree models here used to describe the uncertainties in the geophysical parameters controlling the magnitude-frequency distribution of earthquakes in the source regions reflect our current state of knowledge. Additional scientific information gathered regarding the source regions could potentially change the weightings in the logic-tree and consequently, affect the estimated tsunami hazard (see discussion in Section 3.1).

5.2 Probabilistic Tide-Tsunami Hazard Assessment

Because the PTHA including tidal effects only uses the top 100 tsunami out of approximately 3000 possible tsunamigenic earthquakes that were modelled for the 100 000 year time frame of the Monte Carlo simulations, a legitimate question concerns the possibility that smaller tsunami, outside the top 100 events and therefore not modelled, could cause greater inundation than moderate events if combined with a higher tide. Smaller tsunami could, therefore, significantly alter the results of the probabilistic tsunami-tide analysis.

To assess this, we first created a cumulative plot of all the possible combinations of tsunami wave height (from the 100 largest events) and the varying tidal heights for each point. We found the highest expected sea level in 2500-years (i.e. that sea level that occurs 40 times in 100 000 years). We then considered what proportion of the PDF for the smallest tsunami arrival is larger than this critical value. The percentage of the PDF from the smallest tsunami that lies above the expected 2500-year level provides an indication of the importance of the tidal contribution to inundation at that location; a larger percentage means that a small tsunami may have a significant influence on the probabilistic inundation in the event that it arrives at or around high spring tide. Table 1 illustrates these results: the percentage of the PDF from the smallest tsunami above the 2500-year ARI inundation level is presented together with data on tidal heights and tsunami waves heights at each location for the 100 tsunami scenarios modelled.

Table 1 demonstrates the influence interaction of tidal state and tsunami wave height in determining the ultimate inundation. In areas such as Northcote, Point Chevalier, CBD, Howick, Beachlands, Surfdale and Kaiaua, the PDF percentage exceeds 20%. In these locations, the highest astronomical tide (HAT) is relatively large compared to the other locations, and the height of the tsunami is relatively small. The state of the tide at the time of tsunami arrival, therefore, has a greater influence on the extent of the inundation, and smaller tsunami than were modelled in this study may influence the probabilistic inundation. In other areas, where the highest tide is lower or the tsunami heights are greater, the smaller tsunami have no effect on the calculated probabilistic inundation.

From Table 1 we see that additional tsunami would not make a difference to the results at Omaha and Orewa. The difference would be very small at Snells Beach, Takapuna, St Heliers, Oneroa and Onetangi; small at Whangaparaoa Peninsula and Torbay. However, as noted above, additional tsunami could change results at Northcote, Pt Chevalier, CBD, Tamaki, Howick, Beachlands, Surfdale and Kaiaua. These latter locations tend to be places that are further up harbour and more sheltered from the initial wave.

Table 1

Highest and lowest high tides and highest and lowest maximum tsunami wave heights for points where time series were taken for probabilistic tsunami inundation including tidal heights.

	Area	HAT (m)	Lowest High Tide (m)	Maximum Tsunami Wave Height (m)	Minimum Tsunami Wave Height (m)	2500-year height (m)	Percentage smallest tsunami above
1	Omaha	1.4	0.5	6.2	1.4	4.8	0
2	Snells Beach	1.5	0.6	1.7	0.7	1.9	4
3	Orewa	1.6	0.6	3.0	0.8	2.4	0
4	Whangaparaoa Peninsula	1.6	0.6	1.6	0.7	1.8	14
5	Torbay	1.6	0.7	1.8	0.7	1.9	12
6	Takapuna	1.6	0.7	2.0	0.7	2.0	4
7	Northcote	1.8	0.8	0.9	0.3	1.5	21
8	Point Chevalier	1.9	0.8	0.5	0.2	1.4	33
9	CBD	1.8	0.8	0.9	0.3	1.5	21
10	St Heliers	1.7	0.7	1.7	0.5	1.8	7
11	Tamaki River	1.8	0.8	1.0	0.4	1.6	19
12	Howick	1.7	0.7	0.8	0.4	1.5	23
13	Beachlands	1.7	0.7	0.7	0.3	1.4	24
14	Oneroa	1.6	0.6	2.2	0.7	2.0	9
15	Onetangi	1.6	0.6	2.7	1.0	2.3	5
16	Surfdale	1.7	0.7	0.8	0.4	1.6	28
17	Kaiaua	2.0	0.8	0.4	0.1	1.6	31

It should be noted that the method used here to account for the influence of tidal state on coastal inundation by tsunami does not include dynamic interactions between the tide and the tsunami. For instance, the total water depth is modified by the tidal state during the passage of the wave, as are current speeds and, hence, bed friction. Both effects may modify the propagation and subsequent inundation caused by the tsunami, though probably in relatively minor ways. In order to include these nonlinear interactions, full hydrodynamic modelling of tsunami inundation at all tidal states would be required.

5.3 Limitations of Hydrodynamic Modelling

It is important to understand the limitations of a modelling study. Computer models approximate reality and, inevitably, have shortcoming and limitations. The physics of wave propagation are well understood, and the numerical treatment of the problem by COMCOT and RiCOM has been carefully developed over several years to ensure efficient and accurate simulation. This is demonstrated by the good agreement between the models in predicted

water levels at 175°E. However, tsunami inundation modelling is also dependent on and limited by a number of other factors, in particular the quality of nearshore bathymetry data and LiDAR topography data. Bathymetric data are often relatively sparse and of indeterminate quality, particularly in the coastal zone, and data quality issues are exacerbated by sediment mobility and changing morphology of the nearshore zone. In this study, we have used the best available data for nearshore bathymetry, but there are inherent uncertainties in nearshore modelling caused by poorly known bathymetry.

Other uncertainties include the gridded representation of a continuous coastline, which may deform the shape of bays and estuaries. The effects of building and land features on wave drag are largely unknown, but could substantially modify the onshore propagation of tsunami. Improving the drag representation through use of roughness models remains a goal of current research.

Model uncertainty can be quantified by running multiple simulations with small variations in key parameters, an approach known as ensemble prediction or sensitivity analysis. Such an approach would provide an envelope of predicted solutions, rather than single "worst-case" or "scenario-type" predictions, on which to base emergency response procedures. However, running many simulations increases the computational and research costs. In the current study, computational effort has been used to address the uncertainty in the source of the regional tsunami; performing additional simulations to address uncertainty in the model parameterisations was not a practical option. The largest uncertainty in the modelling process arises from defining the source and generation of the tsunami, and that uncertainty has been addressed in this project in Section 3.1.

Both the models used in this study have undergone quantitative calibration against standard analytical test cases and laboratory benchmark tests. Despite the inherent uncertainties in numerical modelling of tsunami impacts on New Zealand, we believe that the current modelling exercise provides the best possible estimate of inundation of Auckland region from regional source tsunami to date.

5.4 Application of the Results

The modelling of probabilistic tsunami inundation at MHWS provides conservative estimates of probable inundation, and the results may be most appropriate for use in emergency management and planning. The calculations of probable inundation extent incorporating tidal state at the time of tsunami arrival provide a more accurate estimate of probabilistic inundation. It is clear from the analysis in Section 5.2 that incorporating tidal effects increases the potential influence on predicted inundation of small tsunami that were not modelled during the study. Further modelling of these smaller events, and of the dynamic interaction between tides and tsunami, will be required to fully assess the probabilistic inundation from the coupled system.

The predictions of inundation incorporating tidal state presented here serve to illustrate the degree of conservatism in the MHWS approach. The differences between the two approaches vary from location to location, but the MHWS method consistently predicts greater inundation, and the MHWS results are therefore best suited for emergency planning and management in the Auckland region until additional modelling has been performed.

6 Conclusions

A probabilistic tsunami inundation hazard assessment of selected areas on the ARC coast was completed. Subduction zone earthquakes on the Kermadec Arc were the dominant source of regional tsunami impacting the Auckland region east coast for 2500-year ARI exceedances at the 84th percentile of source uncertainty. A simulation of the subduction zone earthquakes that might occur on the Kermadec Arc over a 100 000 year period under the 84th percentile source model was undertaken. The 100 largest tsunami (as determined by their impact on the Auckland region east coast) resulting from the source simulation were selected and the ensuing inundation modelled. The inundation results were then collated to give a probabilistic hazard assessment. Inundation exceedances for tsunami with 2500-year ARI were calculated assuming both a fixed sea level of MHWS and then by explicitly including tidal variation. Maximum speed exceedances for 2500-year ARI tsunami were also calculated, without tides.

The largest impact was on the east coast of Great Barrier Island, although inundation for this area was not explicitly modelled. Omaha Peninsula has a high inundation risk especially on the seaward side. Low lying parts of Orewa, Stanmore Bay and the southern side of the Whangaparaoa Peninsula also have significant inundation risk. In most other areas, the inundation risk is confined to the coastal strip. There is inundation risk to State Highway 1 north of Hatfields Beach and at Northcote and the North-western Motorway between Point Chevalier and Te Atatu. Coastal roads are also at risk of inundation at Devonport and on Waiheke Island. Areas further up the harbour or the Firth of the Thames or sheltered by outlying islands tended to have lower risk of tsunami inundation.

This study presents the first probabilistic analysis of dynamic modelling of tsunami inundation for the New Zealand coast. In all, inundation of the Auckland region from 100 tsunami events has been dynamically modelled, and the results synthesized into probabilistic maps of inundation depth and maximum current speed for tsunami with 2500-year ARI. The simulations conducted assuming tsunami arrival coincides with mean high water spring tides provide conservative estimates of probabilistic inundation suitable for emergency management and planning. Incorporating varying tidal states provides more accurate estimates of the probabilistic inundation, but the results for the present study were hindered because the influence of smaller tsunami on the probabilistic inundation at some locations was not captured in this study. The study provides the most comprehensive assessment of tsunami inundation of the Auckland region from regional source tsunami available to date.

7 References

Abe, K., Estimate of tsunami run-up heights from earthquake magnitudes, in *Tsunami: Progress in Prediction, Disaster Prevention and Warning*, Adv. Nat. Technol. Hazards Res., vol. 4, edited by Y. Tsuchiya and N. Shuto, pp. 21– 35, Kluwer Acad., Norwell, Mass., 1995.

Cho, Y.-S. (1995). Numerical simulations of tsunami and runup. *PhD thesis*, Cornell University, 1995.

Geist, E.L. (2002). Complex earthquake rupture and local tsunami. *Journal of Geophysical Research, 107, B5,* doi:10.1029/2000JB000139.

Goff, J., Pearce, S., Nichol, S.L., Chagué-Goff, C., Horrocks, M. and Strotz, L. (2010), Multi-proxy records of regionally-sources tsunamis, New Zealand. *Geomorphology*, 118, 369-382.

Gonzalez, F. I., Geist, E. L., Jaffe, B., Kanoglu, U., Mofjeld, H., Synolakis, C. E., et al. (2009). Probabilistic tsunami hazard assessment at Seaside, Oregon, for near- and far-field seismic sources. [Article]. *Journal of Geophysical Research-Oceans, 114.*, C11023, doi:10.1029/2008JC005132

Henry, R.F.; Walters, R.A. (1993). A geometrically-based, automatic generator for irregular triangular networks. *Communications in Numerical Methods in Engineering, 9*: 555-566.

Lane, E.M., R.A. Walters, J.R. Arnold, M. Enright and H. Roulston, (2007). Auckland Regional Council Tsunami Inundation Study. NIWA Client Report: CHC2007-126

Liu, P.L.-F., Cho, Y-S., Briggs, M.J., Synolakis, C.E. and Kanoglu, U. (1995). Run-up of solitary waves on a circular island. *J. Fluid Mech.*, 302:259–285, 1995.

Liu, P. L.-F., Cho, Y.-S., Yoon, S. B. and Seo, S. N. (1994). Numerical simulations of the 1960 Chilean tsunami propagation and inundation at Hilo, Hawaii. In *Recent Development in Tsunami Research*, pages 99–115. Kluwer Academic Publishers, 1994.

Mofjeld, H. O., Gonzalez, F. I., Titov, V. V., Venturato, A. J., & Newman, J. C. (2007). Effects of tides on maximum tsunami wave heights: Probability distributions. [Article]. *Journal of Atmospheric and Oceanic Technology, 24*(1), 117-123.

Okada, Y., (1985). Surface deformation due to shear and tensile faults in a half-space, *Bull. Seismol. Soc. Am.*, 75, 1135-1154.

Power, W., Downes, G. and Stirling, M., (2007) Estimation of Tsunami Hazard in New Zealand due to South American Earthquakes, *Pure and Applied Geophysics*, 164 p 547–564

Power, W.L., Wang, X., Wallace, L., & Reyners, M. (2010). Tsunami hazard posed to New Zealand by earthquakes on the Kermadec and southern New Hebrides subduction margins, submitted to *Pure and Applied Geophysics.*

Sadek, E.A. (1980). A scheme for the automatic generation of triangular finite elements. *International Journal of. Numerical Methods in Engineering 15*: 1813-1822.

Staniforth, A.; Côté, J. (1991). Semi-Lagrangian integration schemes for atmospheric models - a review. *Monthly Weather Review 119*: 2206-2223.

Walters, R.A. (2005). A semi-implicit finite element model for non-hydrostatic (dispersive) surface waves. *International Journal for Numerical Methods in Fluid*. *49*: 721–737.

Walters, R.A.; Barnes, P.; Goff, J. (2006a). Locally generated tsunami along the Kaikoura coastal margin: Part 1. Fault ruptures. *New Zealand Journal of Marine and Freshwater Research 40(1)*: 1-17.

Walters, R.A.; Barnes, P.; Lewis, K.; Goff, J., Fleming, J (2006b). Locally generated tsunami along the Kaikoura coastal margin: Part 2. Submarine landslides. *New Zealand Journal of Marine and Freshwater Research 40 (1)*: 18-34.

Walters, R.A.; Casulli, V. (1998). A robust, finite element model for hydrostatic surface water flows. *Communications in Numerical Methods in Engineering 14*: 931-940.

Walters, R.A.; Goff, J.; Wang, K. (2006c). Tsunamigenic sources in the Bay of Plenty, New Zealand. *Science of Tsunami Hazards*, 24, 339-357.

Walters, R. A., Goring, D. G., & Bell, R. G. (2001). Ocean tides around New Zealand. [Article]. *New Zealand Journal of Marine and Freshwater Research, 35*(3), 567-579.

Wang, X. (2008). Numerical modelling of surface and internal waves over shallow and intermediate water. *PhD thesis*, Cornell University, 2008.

Wang, X. and Liu, P. L.-F. (2006). An analysis of 2004 Sumatra earthquake fault plane mechanisms and Indian ocean tsunami. *J. Hydraulic Res.*, 44(2):147–154, 2006.

Wang, X. and Liu, P. L.-F. (2007). Numerical simulations of the 2004 indian ocean tsunami - coastal effects. *Journal of Earthquake and Tsunami*, 1(3):273–297, 2007.

Wang, X., Orfila, A. and Liu, P.L.-F. (2008). Numerical simulations of tsunami runup onto a three-dimensional beach with shallow water equations. p. 249-253 In: Liu, P.L.-F.; Yeh, H.H; Synolakis, C. (eds) *Advanced numerical models for simulating tsunami waves and runup*. Hackensack, NJ: World Scientific. Advances in coastal and ocean engineering 10.

8 Appendix 1: Sensitivity to source location

In response to the draft of this report ARC requested further information on the source properties that influence the impact on the Auckland region. Here we consider the influence of source location along the Kermadec Arc, and how the tsunami impact on the Auckland region varies according to which part of the Kermadec subduction interface is ruptured in an earthquake. The results are presented in Figure A1.

Figure A1
Relative sensitivity of the ARC east coast to earthquake rupture locations along the Kermadec Arc, indicated by the lengths of the horizontal bars.

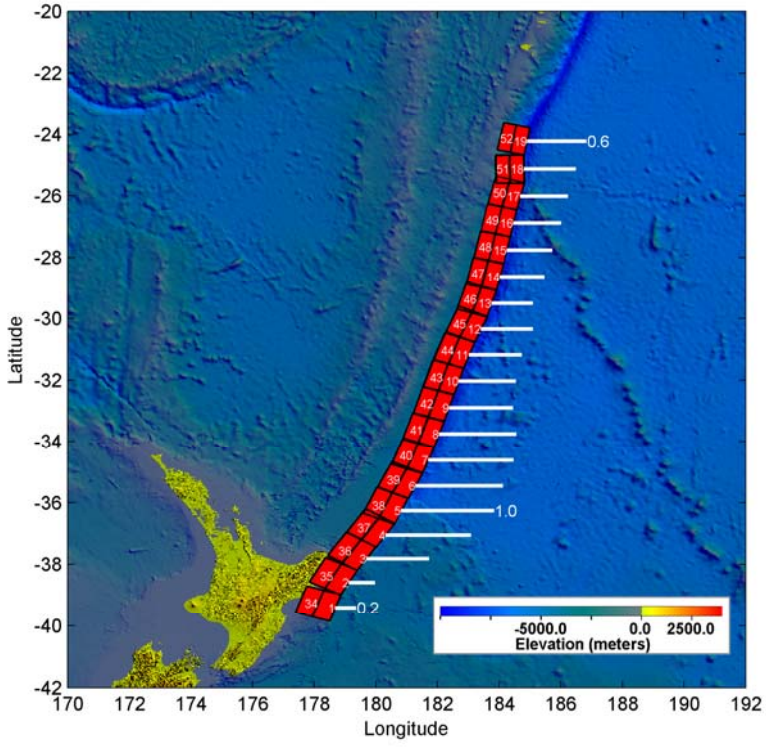

8.1 Method

A 1m slip rupture was considered for each up-dip and down-dip pair of unit source patches, e.g. patches 8 and 41 in Figure A1. Using the unit-source tsunami propagation database, described in Section 3.2, the spatial average (over the ARC east coast shoreline, and extending

to 3km from the coast, but excluding the Barrier Islands) of the maximum tsunami water-level was estimated. These results were normalized relative to the average water-level for the pair of patches with greatest sensitivity, i.e. patches 5 and 38 in Figure A1.

8.2 Discussion

The results shown in Figure A1 demonstrate that the ARC east coast is most sensitive to earthquake ruptures that occur between 100 and 600km north of East Cape. Slip on the plate interface further south is less influential due to the blocking effect of the Coromandel and Raukumara Peninsulas. Slip more than 600km north of East Cape is less influential, by approximately a factor of 2, than that in the high sensitivity region; as most of the tsunami energy is directed further north than the ARC region.

The tsunami scaling laws of Abe (1995) imply that tsunami height approximately doubles for every 0.3 increase in the earthquake moment magnitude. So, loosely speaking, we may expect that, for example, a magnitude 8.3 earthquake located in the high sensitivity region (100-600km north of East Cape) would, on average, have a similar impact to a magnitude 8.6 earthquake located more than 600km north of East Cape. Some caution is required in applying this result, as early estimates of earthquake location often identify the location of rupture initiation, but the ruptures from great earthquakes may extend for hundreds of kilometers from this point.

9 Appendix 2: Maximum wave heights

Table A1. The maximum wave height in metres for each simulation for each of the areas identified in Figure 15 and Table 1. Note that these points are slightly off shore from the areas of interest and that the heights do not include the tidal component.

.	Omaha	Snells Beach	Orewa	Whanga-paraoa	Torbay	Taka-puna	North-cote	Pt Chev-alier	CBD	St Heliers	Tamaki River	Howick	Beach-lands	Oneroa	Onetangi	Surfdale	Kaiaua
1	5.8	1.5	2.6	1.5	1.9	2.0	0.9	0.5	0.9	1.6	1.0	0.8	0.7	2.3	2.7	0.8	0.4
2	5.9	1.7	2.8	1.4	1.8	2.1	0.7	0.4	0.9	1.7	1.0	0.8	0.6	2.3	2.7	0.8	0.4
3	5.7	1.5	2.6	1.5	1.8	2.0	0.8	0.4	0.8	1.6	1.0	0.8	0.7	2.2	2.5	0.8	0.4
4	5.7	1.5	2.5	1.5	1.8	2.0	0.8	0.4	0.8	1.6	1.0	0.8	0.7	2.3	2.6	0.8	0.4
5	5.8	1.7	2.7	1.4	1.7	2.0	0.7	0.4	0.8	1.7	1.0	0.7	0.6	2.3	2.6	0.8	0.3
6	5.5	1.5	2.5	1.4	1.7	1.9	0.8	0.5	0.8	1.5	1.0	0.7	0.7	2.2	2.5	0.7	0.4
7	5.6	1.5	2.5	1.4	1.7	1.9	0.8	0.4	0.8	1.5	1.0	0.7	0.7	2.2	2.5	0.8	0.4
8	5.5	1.5	2.5	1.4	1.7	1.9	0.8	0.4	0.8	1.5	1.0	0.7	0.7	2.2	2.5	0.8	0.4
9	5.4	1.5	2.4	1.4	1.7	1.9	0.8	0.4	0.8	1.5	1.0	0.7	0.7	2.2	2.4	0.7	0.4
10	5.6	1.6	2.6	1.3	1.7	2.0	0.7	0.4	0.8	1.6	0.9	0.7	0.5	2.2	2.5	0.8	0.3
11	5.4	1.5	2.4	1.4	1.6	1.9	0.8	0.4	0.8	1.5	1.0	0.7	0.7	2.1	2.3	0.7	0.4
12	5.4	1.4	2.4	1.3	1.8	1.8	0.7	0.5	0.7	1.4	0.9	0.7	0.6	2.1	2.3	0.7	0.4
13	5.4	1.4	2.4	1.3	1.6	1.9	0.8	0.4	0.8	1.4	0.9	0.7	0.7	2.1	2.4	0.7	0.4
14	5.4	1.5	2.4	1.3	1.6	1.8	0.8	0.4	0.8	1.5	0.9	0.7	0.7	2.1	2.3	0.7	0.4
15	5.3	1.4	2.3	1.3	1.6	1.8	0.8	0.4	0.8	1.5	0.9	0.7	0.6	2.1	2.4	0.7	0.4
16	6.2	1.6	2.9	1.2	1.5	2.1	0.6	0.4	0.7	1.4	0.8	0.8	0.5	2.2	2.7	0.8	0.3
17	5.4	1.4	2.3	1.3	1.5	1.8	0.7	0.4	0.7	1.4	0.9	0.7	0.6	2.1	2.3	0.7	0.4
18	5.3	1.4	2.3	1.3	1.5	1.8	0.7	0.4	0.7	1.4	0.9	0.7	0.6	2.1	2.3	0.7	0.4
19	5.9	1.5	2.7	1.1	1.4	2.0	0.6	0.4	0.7	1.4	0.8	0.7	0.4	2.1	2.6	0.7	0.3
20	5.1	1.4	2.2	1.2	1.4	1.7	0.7	0.4	0.7	1.3	0.9	0.7	0.6	2.0	2.2	0.7	0.3
21	5.2	1.5	2.4	1.2	1.5	1.8	0.6	0.4	0.8	1.5	0.8	0.7	0.5	2.0	2.2	0.7	0.3

.	Omaha	Snells Beach	Orewa	Whanga-paraoa	Torbay	Taka-puna	North-cote	Pt Chev-alier	CBD	St Heliers	Tamaki River	Howick	Beach-lands	Oneroa	Onetangi	Surfdale	Kaiaua
22	5.1	1.4	2.2	1.2	1.4	1.7	0.7	0.4	0.7	1.3	0.9	0.7	0.6	2.0	2.2	0.7	0.3
23	4.3	1.1	1.9	1.2	1.7	1.5	0.5	0.5	0.6	1.1	0.7	0.6	0.5	1.7	1.8	0.6	0.3
24	5.8	1.5	2.6	1.1	1.4	1.9	0.6	0.4	0.7	1.3	0.7	0.7	0.4	2.1	2.5	0.7	0.3
25	5.1	1.4	2.2	1.2	1.4	1.6	0.7	0.4	0.7	1.3	0.8	0.6	0.6	2.0	2.1	0.7	0.3
26	5.0	1.4	2.2	1.2	1.4	1.6	0.7	0.4	0.7	1.3	0.9	0.7	0.6	1.9	2.0	0.7	0.3
27	5.4	1.5	2.5	1.2	1.5	1.9	0.5	0.4	0.6	1.2	0.7	0.7	0.5	2.1	2.2	0.7	0.2
28	4.8	1.3	2.1	1.1	1.4	1.6	0.7	0.4	0.7	1.3	0.8	0.6	0.6	1.9	2.0	0.6	0.3
29	5.6	1.5	2.4	1.1	1.3	1.8	0.5	0.4	0.6	1.3	0.7	0.7	0.4	2.0	2.4	0.7	0.2
30	5.6	1.5	2.4	1.1	1.3	1.8	0.5	0.4	0.6	1.3	0.7	0.7	0.4	2.0	2.4	0.7	0.2
31	4.9	1.3	2.0	1.0	1.4	1.5	0.5	0.3	0.6	1.2	0.7	0.6	0.5	1.9	2.1	0.6	0.3
32	5.5	1.4	2.4	1.1	1.3	1.8	0.5	0.4	0.6	1.3	0.7	0.7	0.4	2.0	2.4	0.7	0.2
33	5.5	1.4	2.4	1.0	1.3	1.8	0.5	0.4	0.6	1.3	0.7	0.7	0.4	2.0	2.4	0.7	0.2
34	4.8	1.3	2.0	1.0	1.4	1.5	0.5	0.3	0.6	1.2	0.7	0.6	0.5	1.9	2.1	0.6	0.3
35	4.8	1.4	2.2	1.1	1.4	1.6	0.6	0.4	0.7	1.3	0.8	0.6	0.4	1.9	2.0	0.6	0.3
36	5.1	1.4	2.4	1.1	1.4	1.8	0.5	0.3	0.6	1.1	0.7	0.7	0.5	1.9	2.0	0.7	0.2
37	4.1	1.1	1.7	1.0	1.6	1.4	0.5	0.4	0.5	1.0	0.6	0.6	0.5	1.6	1.7	0.5	0.2
38	5.1	1.4	2.4	1.1	1.4	1.8	0.5	0.3	0.6	1.1	0.7	0.7	0.5	1.9	2.0	0.7	0.2
39	5.5	1.4	2.4	1.0	1.3	1.7	0.5	0.4	0.6	1.2	0.7	0.7	0.4	1.9	2.3	0.7	0.2
40	4.7	1.4	2.2	1.0	1.4	1.6	0.6	0.4	0.7	1.3	0.8	0.6	0.4	1.8	2.0	0.6	0.3
41	4.6	1.3	2.0	1.1	1.3	1.5	0.6	0.3	0.6	1.2	0.8	0.6	0.5	1.8	1.9	0.6	0.3
42	4.7	1.4	2.2	1.0	1.3	1.5	0.6	0.3	0.7	1.3	0.8	0.6	0.4	1.8	1.9	0.6	0.3
43	4.7	1.2	1.9	0.9	1.3	1.5	0.5	0.3	0.6	1.1	0.7	0.6	0.5	1.8	2.0	0.6	0.2
44	3.4	1.0	1.5	1.2	1.5	1.1	0.4	0.4	0.5	1.0	0.7	0.6	0.4	1.3	1.5	0.5	0.3
45	4.6	1.3	2.0	1.0	1.2	1.5	0.6	0.3	0.6	1.2	0.8	0.6	0.5	1.7	1.8	0.6	0.3
46	5.3	1.4	2.3	1.0	1.2	1.6	0.5	0.3	0.6	1.2	0.7	0.6	0.4	1.9	2.2	0.6	0.2
47	4.9	1.3	2.3	1.1	1.3	1.7	0.4	0.3	0.5	1.0	0.6	0.7	0.5	1.8	1.9	0.6	0.2
48	4.5	1.3	2.0	1.0	1.2	1.5	0.6	0.3	0.6	1.2	0.7	0.6	0.5	1.7	1.7	0.6	0.3

.	Omaha	Snells Beach	Orewa	Whanga-paraoa	Torbay	Taka-puna	North-cote	Pt Chev-alier	CBD	St Heliers	Tamaki River	Howick	Beach-lands	Oneroa	Onetangi	Surfdale	Kaiaua
49	4.4	1.3	1.9	1.0	1.2	1.5	0.6	0.3	0.6	1.2	0.7	0.6	0.5	1.7	1.7	0.6	0.3
50	4.4	1.2	1.8	0.9	1.2	1.4	0.5	0.3	0.5	1.1	0.6	0.6	0.4	1.7	1.8	0.6	0.2
51	4.3	1.2	1.9	1.0	1.1	1.4	0.6	0.3	0.6	1.1	0.7	0.6	0.5	1.6	1.7	0.6	0.2
52	4.3	1.2	1.9	0.9	1.1	1.4	0.5	0.3	0.6	1.1	0.7	0.6	0.5	1.6	1.7	0.6	0.2
53	4.2	1.3	2.0	1.0	1.2	1.4	0.5	0.3	0.6	1.2	0.7	0.5	0.4	1.7	1.8	0.6	0.2
54	3.0	0.9	1.4	1.1	1.3	1.0	0.4	0.4	0.4	0.9	0.7	0.5	0.4	1.2	1.4	0.5	0.2
55	4.8	1.2	2.0	0.9	1.1	1.5	0.5	0.3	0.5	1.1	0.6	0.6	0.3	1.7	1.9	0.6	0.2
56	4.1	1.2	1.8	0.9	1.0	1.4	0.5	0.3	0.6	1.1	0.7	0.5	0.4	1.5	1.6	0.5	0.2
57	2.7	0.8	1.4	0.9	1.1	1.2	0.4	0.5	0.4	0.9	0.7	0.6	0.5	1.1	1.3	0.6	0.2
58	4.1	1.1	1.7	0.9	0.9	1.3	0.5	0.3	0.5	1.0	0.6	0.5	0.4	1.5	1.6	0.5	0.2
59	4.7	1.2	2.0	0.8	1.1	1.5	0.5	0.3	0.5	1.0	0.6	0.6	0.3	1.7	1.9	0.6	0.2
60	4.7	1.2	2.0	0.8	1.1	1.5	0.5	0.3	0.5	1.0	0.6	0.6	0.3	1.7	1.9	0.6	0.2
61	2.6	0.8	1.3	0.9	1.1	1.1	0.4	0.4	0.4	0.8	0.7	0.6	0.4	1.3	1.2	0.5	0.2
62	2.7	0.9	1.3	1.0	1.3	0.9	0.4	0.4	0.4	0.8	0.6	0.4	0.4	1.1	1.2	0.4	0.2
63	2.0	0.8	1.0	0.9	0.9	0.9	0.4	0.4	0.4	0.8	0.7	0.5	0.5	1.0	1.2	0.8	0.3
64	2.7	0.9	1.3	1.0	1.3	0.9	0.4	0.4	0.4	0.8	0.6	0.4	0.4	1.1	1.2	0.4	0.2
65	4.1	1.2	1.9	0.9	1.0	1.4	0.4	0.3	0.5	0.9	0.5	0.6	0.4	1.6	1.6	0.5	0.2
66	2.7	0.9	1.3	1.0	1.2	0.9	0.4	0.4	0.4	0.8	0.6	0.4	0.3	1.1	1.2	0.4	0.2
67	2.5	0.8	1.3	0.9	1.0	1.1	0.4	0.4	0.4	0.8	0.6	0.6	0.4	1.0	1.2	0.6	0.2
68	3.9	1.1	1.6	0.7	1.1	1.2	0.4	0.3	0.5	0.9	0.6	0.5	0.3	1.5	1.6	0.5	0.2
69	3.8	1.1	1.6	0.8	0.9	1.2	0.4	0.3	0.5	0.9	0.6	0.5	0.4	1.4	1.5	0.5	0.2
70	3.8	1.1	1.6	0.8	0.9	1.2	0.4	0.3	0.5	0.9	0.6	0.5	0.4	1.4	1.5	0.5	0.2
71	3.4	0.9	1.4	0.7	1.0	1.1	0.4	0.3	0.4	0.8	0.5	0.5	0.3	1.3	1.4	0.5	0.2
72	3.8	1.1	1.6	0.8	0.9	1.2	0.4	0.3	0.5	0.9	0.6	0.5	0.3	1.4	1.5	0.5	0.2
73	3.8	1.2	1.8	0.8	1.0	1.3	0.5	0.3	0.5	1.0	0.6	0.5	0.3	1.4	1.5	0.5	0.2
74	1.9	0.8	1.0	0.9	0.8	0.9	0.4	0.4	0.3	0.8	0.6	0.5	0.5	0.9	1.1	0.7	0.3
75	2.6	0.8	1.2	1.0	1.2	0.9	0.4	0.4	0.4	0.8	0.6	0.4	0.3	1.1	1.2	0.4	0.2

.	Omaha	Snells Beach	Orewa	Whanga-paraoa	Torbay	Taka-puna	North-cote	Pt Chev-alier	CBD	St Heliers	Tamaki River	Howick	Beach-lands	Oneroa	Onetangi	Surfdale	Kaiaua
76	2.5	0.8	1.2	1.0	1.2	0.9	0.4	0.4	0.4	0.8	0.6	0.4	0.3	1.1	1.2	0.4	0.2
77	2.5	0.8	1.2	0.9	1.2	0.8	0.4	0.4	0.4	0.8	0.6	0.4	0.3	1.1	1.1	0.4	0.2
78	2.5	0.8	1.2	0.9	1.2	0.8	0.4	0.4	0.4	0.8	0.6	0.4	0.3	1.1	1.1	0.4	0.2
79	2.4	0.7	1.2	0.8	1.0	1.0	0.4	0.4	0.4	0.8	0.7	0.6	0.4	1.2	1.1	0.5	0.2
80	2.2	0.8	1.1	0.9	1.0	1.0	0.3	0.4	0.4	0.7	0.7	0.5	0.4	1.2	1.3	0.5	0.2
81	3.3	0.9	1.3	0.7	0.9	1.1	0.4	0.2	0.4	0.8	0.5	0.5	0.3	1.2	1.3	0.5	0.2
82	2.2	0.8	1.1	0.9	1.0	1.0	0.3	0.4	0.4	0.7	0.7	0.5	0.4	1.2	1.3	0.5	0.2
83	4.1	1.1	1.7	0.7	1.0	1.3	0.4	0.3	0.5	0.9	0.5	0.5	0.3	1.5	1.7	0.5	0.2
84	2.4	0.8	1.2	0.9	1.1	0.8	0.4	0.4	0.4	0.8	0.6	0.4	0.3	1.0	1.1	0.4	0.2
85	1.9	0.8	0.8	0.7	0.7	1.0	0.4	0.4	0.3	0.8	0.6	0.5	0.4	1.0	1.1	0.7	0.3
86	3.1	0.9	1.3	0.7	0.9	1.0	0.4	0.2	0.4	0.8	0.5	0.4	0.3	1.2	1.3	0.5	0.2
87	3.6	1.0	1.5	0.8	0.8	1.1	0.4	0.2	0.5	0.9	0.5	0.5	0.3	1.3	1.4	0.5	0.2
88	1.5	0.8	0.8	0.8	0.8	1.0	0.4	0.5	0.3	0.8	0.6	0.5	0.5	0.9	1.1	0.8	0.3
89	2.4	0.8	1.2	0.8	1.0	1.0	0.4	0.4	0.4	0.8	0.7	0.5	0.4	1.0	1.2	0.5	0.2
90	4.0	1.1	1.7	0.7	0.9	1.3	0.4	0.3	0.5	0.9	0.5	0.5	0.3	1.5	1.6	0.5	0.2
91	3.7	1.1	1.7	0.8	0.9	1.3	0.3	0.3	0.4	0.8	0.5	0.5	0.3	1.4	1.4	0.5	0.2
92	4.0	1.1	1.7	0.7	0.9	1.2	0.4	0.3	0.5	0.9	0.5	0.5	0.3	1.4	1.6	0.5	0.2
93	1.8	0.8	0.9	0.7	0.9	0.8	0.3	0.4	0.3	0.6	0.6	0.5	0.4	0.8	1.0	0.5	0.2
94	3.7	1.1	1.6	0.8	0.9	1.3	0.3	0.2	0.4	0.8	0.5	0.5	0.3	1.4	1.4	0.5	0.2
95	2.3	0.8	1.1	0.9	1.1	0.8	0.4	0.4	0.3	0.7	0.5	0.4	0.3	1.0	1.1	0.4	0.2
96	3.5	1.0	1.5	0.7	0.8	1.1	0.4	0.2	0.4	0.8	0.5	0.4	0.3	1.3	1.3	0.4	0.2
97	3.6	1.1	1.6	0.7	0.9	1.1	0.4	0.2	0.5	0.9	0.5	0.4	0.3	1.3	1.4	0.4	0.2
98	1.5	0.6	0.8	0.8	0.8	0.7	0.3	0.4	0.4	0.6	0.5	0.5	0.4	0.9	1.3	0.6	0.3
99	3.9	1.0	1.6	0.7	0.9	1.2	0.4	0.3	0.5	0.9	0.5	0.5	0.3	1.4	1.6	0.5	0.2
100	2.9	0.8	1.2	0.7	0.9	0.9	0.3	0.2	0.4	0.7	0.5	0.4	0.3	1.1	1.2	0.4	0.2